# Development of an Uncompensated Diagnostic for the Measurement of Phase-Resolved Characteristics in Radio-Frequency Plasmas

S. Linnane

January 16, 2008

# Development of an Uncompensated Diagnostic for the Measurement of Phase-Resolved Characteristics in Radio-Frequency Plasmas

*A thesis for the degree of*

## PHILOSOPHIAE DOCTOR

*Presented to*

## DUBLIN CITY UNIVERSITY

*By*

Shane Linnane

School of Physical Sciences

Dublin City University

Research Supervisors:

Dr. Mike B. Hopkins

External Examiner: Dr. John Scanlan

Internal Examiner: Dr. Paul Swift

November 2007

## Declaration

I hereby certify that this material which I now submit for assessment on the programme of study leading to the award of Philosophiae Doctor is entirely my own work and has not been taken from the work of others save and to the extent that such work has been cited and acknowledged within the text of this work.

Shane Linnane, 19th November 2007

# Abstract

In recent years, plasma technology has found its way into a wide and diverse array of manufacturing techniques and facilities, ranging from biomedical applications to microprocessor fabrication. In all cases, greater overall efficiency and usefulness can be improved by understanding the fundamentals of how and why plasmas behave the way they do. In order to achieve this understanding, we use a wide variety of plasma diagnostics to perform measurements of all the important plasma parameters. The work presented in this thesis is focused on electrostatic probes, in particular, the Langmuir probe, which is arguably the most common diagnostic in the world of experimental plasma physics.

Eventhough the Langmuir probe was invented over 80 years ago and was the first diagnostic tool used for studying plasmas in detail, it is still widely used today. The reason it has survived, even in the presence of more accurate and advanced methods, is because no other diagnostic can obtain so many of the important parameters in such a relatively simple way. However, in many cases the Langmuir probe can only be used as an estimator of plasma parameters, as its accuracy is questionable, particularly in radio frequency(rf) discharges. The inaccuracies are caused by the non-linear dynamics of the plasma sheath, which result in an extra dc current component being measured. This extra component, $\Delta I$, results in a difference between the time average I-V characteristic and the effective dc I-V characteristic. In 'normal' operation, the Langmuir probe only measures time averaged values, and so, errors result, such as, over-estimation of electron temperature, $T_e$.

Compensated Langmuir probes have been developed to try and eliminate the distortion effect of the plasma potential oscillation on the probe measurements RF compensation usually involves high impedance inductors placed near the tip and a large compensation electrode, both designed to make the probe tip *follow* the plasma voltage oscillation, thus reducing it impact on the measurements.

Many semiconductor processing tools use capacitively coupled plasma discharges (CCP's) for etching, deposition and sputtering. CCP's generally have a large voltage oscillation so the ability to accurately measure the plasma parameters under these conditions is highly desirable. Unfortunately, even highly compensated probes have difficulty in providing accurate measurements under most CCP conditions. This is because, in practice, it is very difficult to achieve sufficient probe impedance relative to the sheath impedance and also probe construction can be difficult, especially for commercial discharges. For these reasons, and others, even compensated probes do not give reliable results in plasmas with large voltage oscillations.

This was the main motivation for the work presented in this thesis - to design a probe capable of accurately measuring the I-V characteristics and plasma potential oscillations without the need for complex compensation techniques. To achieve this goal, a simple uncompensated Langmuir probe was investigated. A computer model was constructed in MatLab to aid in the understanding. A technique was developed in which the *distortion-free* I-V characteristic is obtained from the time-averaged (distorted) I-V trace by utilizing the rf data measured through a capacitively-coupled, synchronized rf current sensor. This allows phase dependant characteristics to be obtained and also allows reconstruction of the plasma potential oscillation, complex sheath impedance and other important properties.

The probe design and circuitry are relatively simple, thus providing a useful diagnostic for probing radio-frequency plasmas.

# Acknowledgements

First of all I would like to thank my supervisor, Dr. Mike Hopkins, for his support, ideas and enthusiasm, which made the task much less painful.

I would also like to thank the other staff members who I have learned a great deal from and helped who me out along the way, Dr. Bert Ellingboe, Prof. Miles Turner, Dr. Ronan Faulkner, and Dr. Bernard Keville and others too numerous to mention, and to the administration staff, Sam, Sarah, Sheila and Lisa.

Thanks to all the fellow post-grad students who I had many useful (and many not so useful !) conversations with. These include Chanel, Derek, Dave, Angus, Peter S, Peter B, Mohammad, Deberah, Felipe, Niall, Cezar, Bernard, Andrew and again others too numerous to mention. Without their support, on both a personal and academic note, I don't think I would have survived!

Thanks to Chanel for putting up with me, especially when my experiments weren't going too well - which was most of the time. You are clearly

1

very patient ! Thanks for everything.

And last but not least, thanks to my parents for their unconditional support for nearly 30 years, which is about 12 years more than the standard parenting contract. Without their hard work I would not have had the chance to experience the relatively easy life of a perpetual student. Thank you. Also I should probably say sorry to my younger sister and brother, Lyndsey and Ryan, as you are now both expected to follow in my glorious foot-steps ! But I don't think that will be a problem for either of you.

# Contents

# CONTENTS

# List of Figures

# CHAPTER 1

---

## Overview

---

The aim of this thesis is to present an uncompensated electrostatic probe technique that is capable of accurately measuring phase-dependant I-V characteristics in radio-frequency plasmas.

In rf plasmas, the probe current, I, is a function of both the applied dc probe voltage, $V$, and the oscillating sheath voltage at the probe tip, $\tilde{V}_{sh}$, which is a function of time, t, i.e.

$$I(V, \tilde{V}_{sh}, t) \tag{1.1}$$

where $\tilde{V}_{sh} = \tilde{\Phi}_p - V$ and the total plasma potential, $\tilde{\Phi}_p$ is given by

$$\tilde{\Phi}_p = \overline{\tilde{\Phi}}_p + \tilde{\Phi}_{p_{rf}} \tag{1.2}$$

where $\overline{\tilde{\Phi}}_p$ is the time-averaged plasma potential and $\tilde{\Phi}_{p_{rf}}$ is the oscillating component of the plasma potential, at the driving frequency, $f_{dr}$.

The effective dc characteristic, $I_{DC_{eff}}$, is found at t = 0, i.e. $I_{DC_{eff}}(V) = I(V, 0, 0)$. Experimentally however, an uncompensated probe only has sufficient temporal resolution to measure the time-averaged current, $\overline{I}(V) = I_{ave}(V)$, which has a distortion component $\Delta I(V)$. Therefore, calculating the important plasma parameters from $I_{ave}(V)$ results in distorted values, such as, over-estimation of electron temperature, $T_e$, and underestimation of electron density, $n_e$.

$$\overline{I}(V) - I(V, 0, 0) = \Delta I(V)$$
$$\Rightarrow \overline{I}(V) - \Delta I(V) = I(V, 0, 0) \qquad (1.3)$$
$$\Rightarrow I_{ave}(V) - \Delta I(V) = I_{DC_{eff}}(V)$$

Up until the present time, rf compensation has been the only widely accepted method available for obtaining $I_{DC_{eff}}(V)$, but for large oscillation amplitudes sufficient compensation is very difficult to achieve, and so, the measured characteristic is usually a distorted version of $I_{DC_{eff}}(V)$. It will be shown that there is a fundamental link between the sheath generated harmonics and $\Delta I$, thus allowing $I_{DC_{eff}}(V)$ to be measured accurately without rf compensation. This also leads to a more powerful method which allows the phase-dependant characteristics to be determined.

By separating the dc and ac current components, through a slight modification of the conventional Langmuir probe circuit, and utilising a phase reference at the fundamental of $f_{dr}$, it can be shown that

$$\tilde{I}_{rf}(V, \tilde{V}_{sh}, t) \Rightarrow \tilde{I}_{rf}(V, \tilde{V}_{sh}, \phi) \qquad (1.4)$$

where $\tilde{I}_{rf}$ is is the measured a.c. current component and $\phi$ is the phase relative to the driving oscillation. Thus, importantly,

$$I(V, \tilde{V}_{sh}, \phi) = \overline{I}(V) + \tilde{I}_{rf}(V, \tilde{V}_{sh}, \phi) \tag{1.5}$$

From $I(V, \tilde{V}_{sh}, \phi)$, we obtain $I_{DC_{eff}}$ at $I(V, 0, 0)$, while also the phase-dependant plasma parameters are measurable, such as, $n_e(\phi)$, $T_e(\phi)$, $\tilde{\Phi}_p(\phi)$ and $f(E, \phi)$ (the electron energy distribution function).

With present methods, these parameters are generally not measurable at high frequencies, thus, this new technique opens up many possibilities and allows a deeper investigation of rf plasmas with a simple uncompensated probe.

# CHAPTER 2

---

## Introduction

---

At the turn of the 19th century, electrical discharges were already being used for various purposes, including lighting applications, but a more detailed study of their behaviour only came about around 1924 [1]. It was in this year that Irving Langmuir and Mott-Smith published their work describing a new technique and theory for interpreting the I-V characteristic of a low pressure plasma [2]. This was the beginning of detailed scientific investigation of the plasma state and the birth of accurate plasma diagnostics [3].

Today, plasma processing is commonplace in many industrial applications, the best known of which is in the fabrication of microelectronics. With the ever-decreasing scale of surface features on etched wafers, the need for greater control and accuracy must be matched by our ability to accurately measure the plasma parameters. The role of plasma diagnostics is crucial in this. One of the major advantages of electrostatic probes is that they

can provide localized measurements, unlike most other diagnostics, of which there are many, for example, microwave interferometry, laser induced fluorescence and cavity ring-down spectroscopy to name but a few. However, even with the plethora of elaborate diagnostics available, the 'simple' Langmuir probe is often used as a seemingly easy measure of many of the important plasma parameters.

However, many of todays industrial plasma processors use RF generated plasmas, which Langmuir's original analysis was never intended for. The oscillation of the plasma potential causes an oscillating probe current, the time-average of which does not equal the dc current (without oscillation), thus, the measured characteristic is distorted. Rf compensation techniques have been developed to reduce or eliminate the erroneous effects of the oscillation. In reality, however, the compensation techniques are difficult to implement, particularly for plasmas with large oscillations [4][5] Despite the difficulties, compensated Langmuir probes are often used as estimators of plasma parameters or indictors of change in operating conditions.

## 2.1   The Langmuir Probe

The probe itself is simple, consisting of a shielded wire, exposed only at one end to the plasma. The exposed probe tip is usually made from a high melting point conductor, such as tungsten. The tip is biased by a variable voltage source through a low impedance resistor. An I-V characteristic of the plasma is obtained by recording the current through the resistor as a function of bias voltage.

From the I-V characteristic, the important plasma parameters can be determined, such as, the electron temperature, $T_e$, ion and electron densities, $n_i$

and $n_e$ respectively, floating potential, $V_F$ and time-averaged plasma potential, $\overline{\Phi}_p$ [6–8]. The electron energy distribution function (EEDF) can also be obtained. The I-V characteristic can be divided into three distinct regions; ion saturation, exponential region and electron saturation. Each of these regions will be discussed in turn, but first we will take a brief look at the development of probe theories used to interpret the plasma I-V characteristic.

### 2.1.1 Probe Theory

Measuring the I-V characteristic is relatively easy, but interpreting how this characteristic is related to the plasma parameters is far more difficult. Langmuir and Mott-Smith were the first to develop a basic theory which attempted to bridge this gap. However, even today, over 80 years after their work, a completely general theory of current collection to probes still does not exist.

The simplest approach to probe theory is to assume a Maxwell-Boltzmann electron velocity distribution, to neglect plasma disturbance by the probe and particle collision effects, and to assume a completely absorbing probe, i.e. every attracted particle that enters the sheath is assumed to be collected. Under these conditions, the total current, $I$, in the electron retarding region of the I-V curve, i.e. below the plasma potential, is given by

$$I = -I_{ion} + I_{e_{sat}} exp\left( -\frac{\Phi_p - V_{bias}}{T_e} \right) \qquad (2.1)$$

where; $I_{ion}$ is the constant ion current and the negative sign indicates positive ion collection. $I_{e_{sat}}$ is the saturation electron current which decreases exponentially for sheath voltage, $V_{sh} < 0$, where $V_{sh} = \Phi_p - V_{bias}$. $T_e$ is in electron volts.

For an ideal planar probe, whose sheath width expands with sheath volt-

age, but sheath area remains constant, the collection area of the probe does not change throughout the I-V characteristic, and so, the electron and ion saturation currents are given respectively by,

$$I_{e_{sat}} = \frac{1}{4}en_oA_p\bar{v}_e \tag{2.2}$$

and

$$I_{ion_{sat}} = -en_sA_pv_B \tag{2.3}$$

where, $A_p$ is the probe collection area, $n_o$ is the plasma density ($n_o = n_e = n_i$), $n_s$ is the sheath edge density, which is approximately 0.61 times $n_o$ [9]. $\bar{v}_e$ is the average thermal velocity of the electrons ( $= \sqrt{8eT_e/\pi m_e}$). $v_B$ is the Bohm velocity, given by,

$$v_B = \sqrt{eT_e/M_{ion}} \tag{2.4}$$

where, $M_{ion}$ is the ion mass, $T_e$ is in eV.

Equation 2.4 is valid for $T_{ion} << T_e$. The sheath edge is often defined as the point at which the ions reach $v_B$, after gaining energy in the presheath. $n_e$ must always be less than $n_{ion}$ within the sheath, so this energy gain in the presheath is necessary in order for the current fluxes to balance.

Equation 2.1 shows that the total current collected by the probe is a combination of ion and electron current. For $V_{bias} < \Phi_p$, the ion current to the probe is essentially constant (so $I_{ion_{sat}} = I_{ion}$). When $V_{sh} > 0$, i.e. when the bias voltage goes above the plasma potential, the electron current is no longer an

exponential function of voltage as it begins to saturate. The current above $\Phi_p$ is thus given by equation 2.2.

Equations 2.2 and 2.3 are only valid for an ideal planar probe, whose sheath width varies as a function of bias, but collection area remains constant. Most probes for plasma research are cylindrical in nature, due to simplicity of construction and less of a perturbation effect than planar probes [10]. In reality, the planar sheath tends to take on a hemispherical shape at large voltages [10], thus causing non-ideal results. For cylindrical probes, the collection area is a function of sheath voltage. As the collection area grows with bias, the current tends not to saturate as it does in the ideal planar case, but instead, increases approximately as a square-root dependance on $V_{sh}$ The effective collection area of a cylindrical probe, $A_{eff}$, is given by,

$$A_{eff} = A_p[1 + (d_{sh}/p_r)]; \qquad (2.5)$$

where $A_p$ is the probe tip area, $p_r$ is the probe tip radius and $d_{sh}$ is the sheath width given by Child's law [9],

$$d_{sh} = \frac{\sqrt{2}}{3}\lambda_D \left(\frac{2V_{sh}}{T_e}\right)^{\frac{3}{4}} \qquad (2.6)$$

where $\lambda_d$, the Debye length, is given as $(\epsilon_o T_e / e n_s)$ and $n_s$ is sheath edge density.

Equations 2.2 and 2 3 therefore need to be modified for cylindrical probes so that sheath expansion is taken into account. The fact that the sheath expands with $V_{sh}$ is a good demonstration of the collective behaviour of plasmas, as the sheath changes to shield out the increasing electric field from reaching the quasi-neutral bulk plasma.

For large negative biases equation 2.6 is valid, so when used in combination with (2.5) and substituted into (2.3), an approximate value for the ion saturation can be obtained. However, a more valid equation to use is that of Laframboise [11], which has been parameterized by Steinbrüchel [12] as,

$$I_{ion} = en_{ion}A_p\sqrt{eT_e/2\pi M_{ion}}\left[a\left(\frac{e(\Phi_p - V_{bias})}{T_e}\right)^b\right] \qquad (2.7)$$

The term in square brackets is essentially a correction factor to the saturation ion current, where the values 'a' and 'b' depend on the ratio of $r_p/\lambda_D$. For cylindrical probes, with $r_p/\lambda_D < 3$, $a$ and $b$ can be approximated by 1.13 and 0 5 respectively [10].

Equation (2.7) gives the orbital motion limited ion current to a cylindrical probe in a collisionless, Maxwellian plasma. Orbital motion limited(OML) theory, was originally developed by Mott-Smith and Langmuir [2] to take account of the fact that for cylindrical probes, ions entering the sheath with a particular angular momentum may actually miss the probe, even-though they are attracted to it. The effects of collisions are ignored  A sheath is generally considered collisionless if the sheath thickness, $\Delta d_{sh}$ ($= d_{sh}$ - $r_p$) is less than the mean free paths of either ions, $\lambda_{ion}$, or electrons, $\lambda_e$.

Laframboise [11] extended this model to include the shape of the electric potential distribution in the sheath and presheath, which depends on the ratio of ion to electron temperature. This provides an exact numerical solution to the equations governing ion collection in collisionless sheaths. Laframboise calculated ion and electron saturation currents for various ratios of $(r_p/\lambda_{De})$, assuming a non-collisional sheath. Equation (2.8) gives the electron saturation, where again, the terms in brackets represent a correction factor for the sheath expansion and the coefficients $\beta$ and $\gamma$ depend on the ratio $r_p/\lambda_D$.

$$I_e = en_e A_p \sqrt{eT_e/2\pi M_e} \left[ \beta \left( \frac{e(\Phi_p - V_{bias})}{T_e} + 1 \right)^\gamma \right] \qquad (2.8)$$

There is still some controversy over the range of applicability of this theory. It is known [6, 7, 10] that Laframboise theory may overestimate ion densities even in the presence of very weak collisionality. This is due to the destruction of ion orbits. This theory therefore gives an upper limit to the collected ion current in the low pressure regime. The electron collection is not nearly as affected by collisions, due to the higher temperature and mobility of the electrons. Also, electron current is collected near the plasma potential where the sheath width may be vanishingly small, so sheath expansion effects have less influence. For theses reasons, electron currents calculated with Laframboise theory can be considered much more accurate over a wider range of applicability than the ion current. Ions are therefore more likely to be affected by sheath expansion effects and collsionality, necessitating a more complex theory. Electron densities calculated from this theory are accurate up to about 20 mTorr. This has been shown in many publications, [7, 10, 13, 14], by comparing the measured ion and electron densities in quasi-neutral plasmas. The calculated ion densities however, are higher, even under conditions where Laframboise theory is expected to be valid, i e.

$$d_{sh} << (\lambda_{ion}, \lambda_e), \lambda_{De} << (\lambda_{ion}, \lambda_e) \text{ and } (r_p/\lambda_{De}) < 3.$$

Allen-Boyd-Reynolds(1957)[15] proposed the radial ion motion theory, which assumes the ions fall freely to the probe following radial paths. $T_{ion}$ is taken as zero and angular momentum effects are ignored. Because orbital effects are neglected, this theory does not suffer as much from the effects of collisions. Experimental results for ion currents are better than those from

Laframboise theory, but may still be overestimated by a factor of 2 [10]. However, the fact that this theory appears to give more realistic ion current values, does not necessarily mean that its physical picture is the correct one. Chen [5] gives reasons as to the validity of this radial motion theory over the orbital motion type theories of Langmuir and Laframboise.

Recent work by Pletnev and Laframboise [16] has re-examined the original theory of Laframboise [11], extending it to include collisions within the sheath. Charge exchange collisions, elastic ion-neutral collisions and elastic/inelastic electron-neutral collisions are considered. They have compared their theoretical results to the experimental data of Sudit and Woods [10], which showed that collisionless theory breaks down when $\lambda_{ion} \sim d_{sh}$. The new collisional theory is in agreement, however, it predicts that breakdown occurs much sooner, i.e. even when $\lambda_{ion} > d_{sh}$ collisional effects can dominate. They found that the validity of the original Laframboise collisionless theory is not guaranteed by the conditions $d_{sh} << \lambda_{ion}$ or $r_p << \lambda_{De}$ because the path lengths can be greatly increased by angular momentum conservation between collisions. An increase in trajectory length also increases the probability of collision. Collisions thus play a more important role, even in conditions where they would not previously have been expected. Also, an increase in sheath width allows more orbital paths to become possible and increases the average trajectory length, thus the possibility of collision is further increased. Very long trajectories, representing quasi-trapped ion orbits, increase the ion density in the sheath, leading to a sharper potential variation. This collisional model also shows that the potential distribution of the sheath does not change significantly when angular momentum effects are removed, but the density of ions near the probe is greatly increased. This may help explain why radial motion theories give higher, apparently more

accurate, ion currents (under certain conditions).

Provided the probe potential does not exceed 40V positive or negative, collisionless theory has been shown to be valid for electron current measurements over a wide range of densities [6, 7, 10]. For the ion currents to be correctly determined from collisionless theory, assuming the pressure is less than 20 mTorr, the density must be sufficiently high. In all other cases, collisional effects must be included. This can be partially explained by the fact that higher density gives a smaller sheath width and since the sheath width is an important collisionality parameter, both density and applied bias may alter the range of applicability of collisionless theory.

So, after many years of investigation, there is still no single theory which can be simply applied in all situations, however, this new collisional theory of Pletnev and Laframboise [16] seems to offer the most accurate solution to date.

## 2.1.2  I-V characteristic: Ion Saturation Region

Figure 2.1 shows the I-V characteristic of an ideal planar probe and also, the more typical, non-ideal characteristic of a cylindrical probe.

When the probe is biased negatively with respect to the plasma potential, positive ions are attracted and electrons are repelled. For a perfect planar probe, where collection area is not a function of bias voltage, the ion current is essentially constant for $V_{bias} < V_{plasma}$. At sufficiently large negative potentials, the measured current will be entirely from ions as the electrons do not have sufficient energy to cross the sheath and get collected by the probe. A further increase in bias will not increase the collected current, i.e. the ion current saturates.

In practice however, we rarely see this saturation condition exactly as
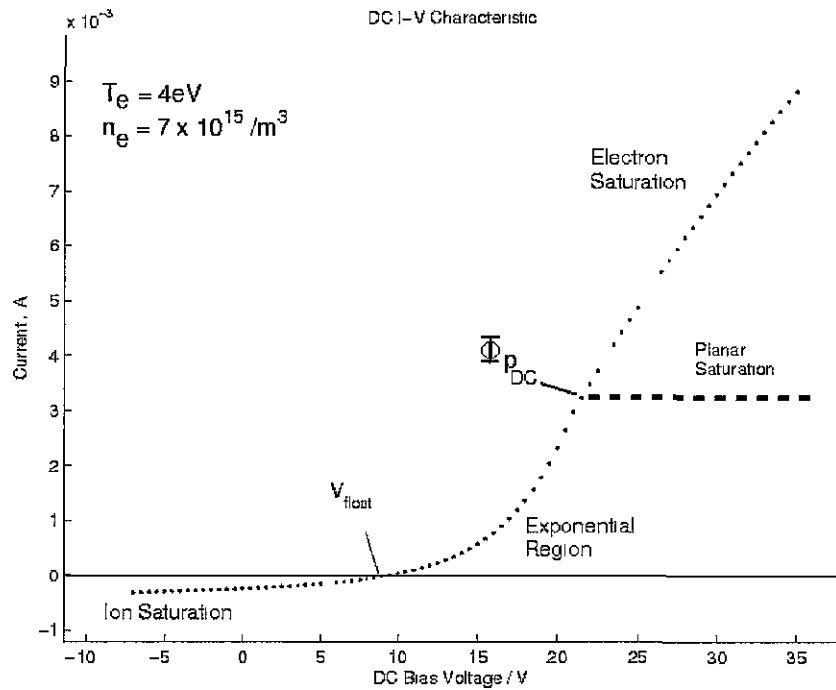
**Figure 2.1:** *I-V characteristics for planar and cylindrical Langmuir probes*

planar probes suffer from edge effects and also hemispherical distortion of the sheath edge as a function of bias voltage. *Guard rings* are often used to reduce edge effects, thus, allowing planar probes to produce I-V characteristics with more complete saturation regions. Great care is needed in their construction to ensure this experimentally.

For cylindrical probes, the sheath radius, and consequently the sheath area, changes as a function of bias voltage, thus collection area changes. Cylindrical probes are easier to construct and were used in all the experimental data presented in this thesis. For that reason, we will only discuss cylindrical probes for the remainder of this thesis, unless stated otherwise. Because $A_{eff}$ increases with bias, as saturation is approached the collection area grows and more current is collected, thus incomplete saturation is

achieved.

Using ion saturation current, $I_{ion_{sat}}$, we can estimate the ion density, from equation (2.3), assuming we know $T_e$ and $m_i$. However, in order to measure $T_e$ accurately, we must first subtract $I_{ion_{sat}}$ from the exponential region of the I-V characteristic. Fitting the data to a theoretical curve is perhaps better [7] [17].

### 2.1.3 I-V characteristic: Exponential Region

If the probe is in ion saturation and the sheath voltage is reduced, i.e. if the bias voltage is made more positive with respect to the plasma, initially, only the higher energy electrons may have enough thermal velocity to penetrate the sheath completely and get collected by the probe. As $V_{sh}$ is reduced further, more and more of the electrons will have enough energy to overcome the reduced repulsion of the sheath. At some point in bias, depending on the exact shape of the electron energy distribution function, the majority of electrons will make it to the probe. Because electrons have a much higher thermal velocity than the ions, it is the electron current that dominates. Ions are still being collected at approximately the same rate as in ion saturation, however, their signal is swamped by the larger electron current.

A small change in bias voltage (2-3 volts) can drastically effect the number of electrons collected by the probe. The electron current is an exponential function of bias voltage. The exponential region can be used to calculate the mean electron temperature. This is done by first subtracting $I_{ion_{sat}}$ from the total measured current to reveal only electron current. A semi-log plot of electron current versus bias voltage yields a straight line in the electron retardation region (assuming a maxwellian distribution). The inverse of the slope of this line gives $T_e$ in electron volts (eV). The $T_e$ calculated from this

method is clearly very sensitive to the exact shape of the exponential region of the I-V characteristic. Anything that alters this region will drastically affect the accuracy of the measurement, such as, a deviation from a Maxwellian distribution or the effects of time averaging an oscillating current (section 2.2). For the collisional case (higher pressures), the electron current may change more slowly with bias than exponential. In this case, the semi-log plot will not be linear making $T_e$ measurement less accurate. In this situation, diffusive models like that of Rozhanski[17] and Strangby[18] may be applied to reveal the correct electron temperature. It should be noted here that $T_{ion}$ should in principal be measurable in a similar way, but in reality we are limited by the fact that $T_e \gg T_{ion}$, and because $I_{ion}$ is only weakly dependant on $T_{ion}$.

## 2.1.4   I-V characteristic: Electron Saturation Region

As the bias voltage approaches the plasma potential, the sheath voltage approaches zero. At $V_{bias} = \overline{\Phi}_p$ , the probe is at the same potential as the plasma, so no sheath forms (at least in a dc plasma). The collection area then becomes that of the probe tip area. Because there is no sheath, electrons and ions are neither attracted nor repelled, they simply collide randomly against the probe tip. Again, because of the higher thermal velocity of the electrons, it is $I_e$ that dominates.

As the bias is increased further, the probe looks positive with respect to the plasma and so electrons are attracted while ions are repelled. Equation 2.8 can be used to calculate the saturation electron current as a function of bias in this region.

The transition from exponential to the $I_{e_{sat}}$ region also marks the position of the plasma potential. This is usually seen as a 'knee' in the curve, (see

figure 2.1). In a dc plasma, the knee can be quite distinctive, so $\overline{\Phi}_p$ can be determined easily and accurately, however, as we will see later (section **2.2**), in an RF plasma this is generally not as easy. $\overline{\Phi}_p$ is determined by a linear extrapolation from the electron saturation region and an extrapolation from the exponential region. The point at which they cross is $\overline{\Phi}_p$. This may be somewhat easier to identify on a semi-log plot. It can also be identified by the peak of the first derivative, or the zero crossing point of the second derivative, of the I-V characteristic. In theory, the second derivative should have positive and negative peaks, both at, or at least very close to, the zero crossing point. In practice, very high signal-to-noise ratio is required to obtain accurate second derivatives. This is usually accomplished by a large number of averages per point.

Another method for directly obtaining the second derivative will be described, in section 3.2, where an accurate second derivative is important, as it can also be used to calculate the EEDF, via the Druyvestyn equation. The integral of the EEDF gives $n_e$, and using this, the effective electron temperature can also be obtained. This method of determining both $n_e$ and $T_{eff}$ has a number of advantages, such as, it is valid for any convex probe geometry [19] and for any isotropic electron velocity distribution, it can measure non-Maxwellian distributions and it is not dependant on the ratio $r_p/\lambda_D$ or $T_{ion}/T_e$ [20]. The EEDF method is often assumed to be the most accurate method [6, 17], however it requires $\overline{\Phi}_p$ to be known accurately, which may be difficult to determine from the I-V characteristic, especially in the presence of rf.
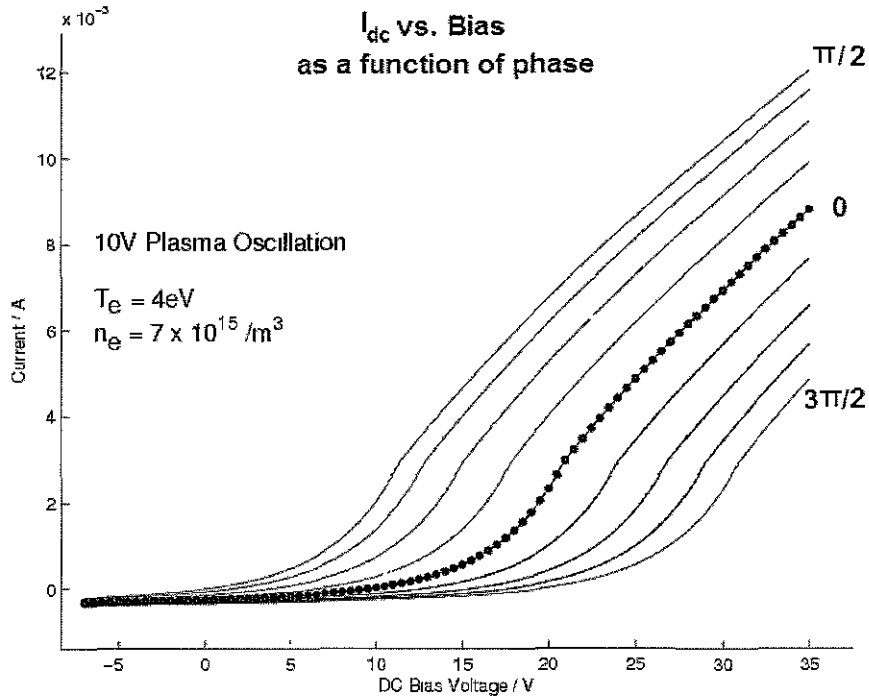
**Figure 2.2:** *Simulated phase-dependant I-V characteristics with plasma potential oscillation of 10V.*

## 2.2 Time-averaged distortion

If the measured current to the probe is time dependant, then the time-averaged I-V characteristic will not appear as it does at t = 0. The 'shape' of the curve, and consequently the calculated parameters, suffer from distortion. This is probably the largest single source of error for Langmuir probe traces in plasmas with oscillating voltages.

In a rf plasma, the probe will be swept by the plasma potential oscillation amplitude at the driving frequency of the plasma source. Because this frequency is generally in the megahertz range, the probe experiences many rf cycles at each dc bias point in the I-V characteristic. Figure (2.2) illustrates how the I-V characteristic changes as a function of phase.
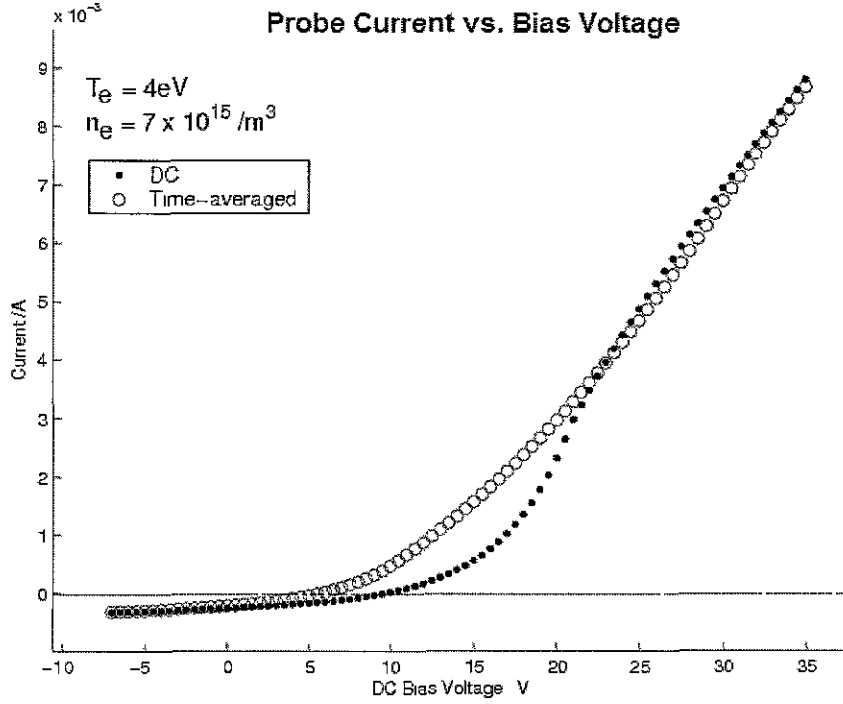
**Figure 2.3:** *Simulated time-averaged trace(circles) compared with dc characteristic(dots). The average is calculated from figure 2.2, where the oscillation amplitude is 10V*

The non-linear nature of the sheath means that the time average of this oscillating trace does not equal the dc (or t = 0) trace. In a conventional Langmuir probe set-up, only the time averaged values are measured, and so, in the case of rf plasmas, we get a distorted characteristic (See figure 2 3). The distortion factor increases with the ratio $(\tilde{\Phi}_{p_{rf}}/T_e)$ [21]. When the ratio is less than unity, the distortion is generally negligible, at least for calculation of $T_e$. The source of the problem is that the non-linearity causes an extra current component, $\Delta I$, for a given dc bias voltage. This extra current is added to the *normal* dc probe current.

If the current is averaged over one period of oscillation, the resultant is not

## Log ($I_e$) vs. Bias Voltage
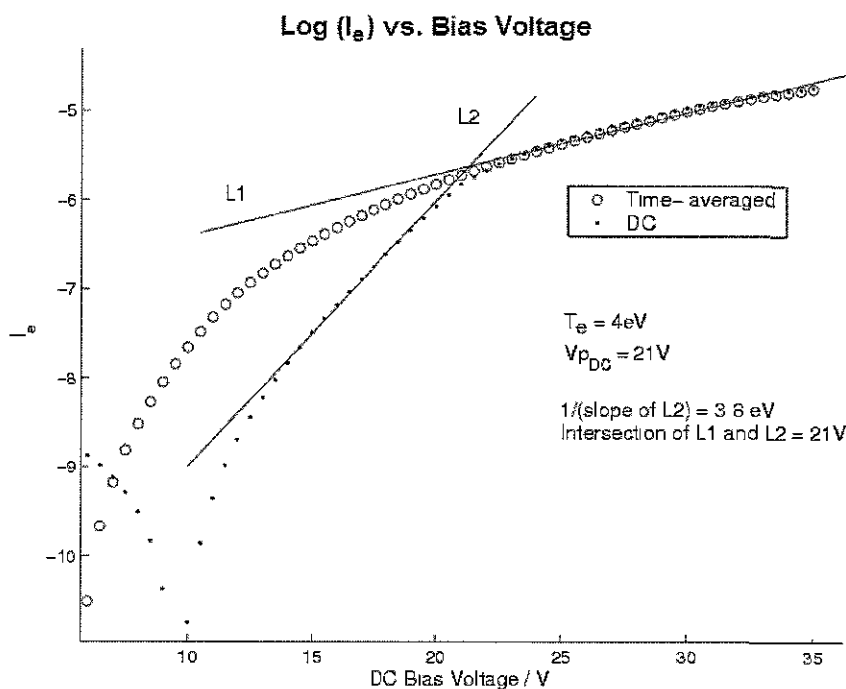


**Figure 2.4:** *Simulated $T_e$ measurement with DC Characteristic. The time-averaged trace is shown for comparison. L1 and L2 are linear fits. The DC trace yields the correct dc plasma potential and approximately correct $T_e$ values, whereas the same procedure on the time-averaged trace would return a serious error on both measurements.*

equal to the t = 0 (effective dc) trace, as shown by figure 2.3. The resultant time-averaged trace appears more linear than the dc trace, particularly in the exponential region. This leads to serious over-estimation in the calculation of $T_e$, as shown in figure 2.4.

So called *rf compensation* techniques have been developed to combat the source of this time-averaged distortion.

## 2.3    Compensated Langmuir Probes

In order for the I-V data collected from a Langmuir probe to be interpreted accurately , either the distortion has to be taken into account in the analysis of the data [22], or the source of the distortion must be eliminated. To date, most authors have taken the second option, by trying to eliminate or reduce the amplitude of oscillation experienced by the sheath.

One of the most common methods is to employ high impedance inductors as close to the probe tip as possible. This was first shown by Gagne and Cantin [23]. The idea is to make the oscillating voltage drop across the inductor, as opposed to the sheath, in an rf voltage divider type arrangement. By doing so, the sheath oscillates to a smaller extent, resulting in a smaller amplitude oscillation in collected current. Effectively, the probe *follows* the oscillation, thereby reducing its impact. The dc currents can still flow as the inductors should have a relatively low dc resistance.

In order for this to work in practice we must therefore have an inductor impedance, $Z_L$, much greater than the sheath impedance, $Z_{sh}$. Chen [4], and Godyak [24] show that the conditions for sufficient compensation are:

$$\mid Z_{sh}/Z_{circuit} \mid < (0.3 - 0.5)T_e/\tilde{\Phi}_{p_{rf}} \qquad (2.9)$$

where $Z_{circuit}$ is the total impedance of the probe and circuitry combined, thus includes $Z_L$ and any stray capacitances.

Using this equation, with $T_e = 4\text{eV}$, $\tilde{\Phi}_{p_{rf}} = 20\text{V}$, the circuit impedance must be approximately 32 times the sheath impedance. Assuming a sheath impedance which is dominated by a 1.0 pf capacitance, then $Z_{circuit}$ must exceed about 380 kΩ at 13.56 MHz. At 27.12 MHz, this required impedance is reduced by a factor of 10. Achieving this is very difficult, and becomes

more difficult as $\tilde{\Phi}_{p_{rf}}$ increases.

In order to achieve such high impedances, high Q-factor, self- resonant inductors are used [25–27]. These may be frequency tuned slightly by adding external capacitance, but generally at the expense of impedance. Because the desire is for high impedance, we need a high Q-factor to achieve this. The difficulty here is that a high Q-factor implies a very sharp rise of impedance over a very narrow frequency range so if the inductor becomes de-tuned for whatever reason, the impedance at the desired frequency may be significantly reduced.

Tuned inductors are extremely sensitive to stray capacitance. This is evident from the fact that placing a tuned inductor inside the ceramic shield of the probe can significantly alter its resonant frequency, thereby changing its impedance. Similarly, the probe may experience a difference in capacitance to ground when the plasma is on as opposed to when it is off. Building in-situ variable inductors is very difficult.

Also, if the inductors are placed near the probe tip, they will be exposed to variations in temperature, which again can significantly change the impedance. In-situ cooling of the inductors is possible, but difficult and complicated to achieve. Another obvious problem is in getting the inductors as close to the tip as possible, while also maintaining a small probe cross section.

Because of the problems associated with generating a high rf impedance on the probe, *compensation electrodes* can also be used in conjunction with inductors. Compensation electrodes are basically large surface-area conductors attached to the probe, in contact with the plasma. They are capacitively coupled to the probe tip so they do not add to the measured dc probe current. The compensation electrodes simply increase the surface area of the sheath from an rf point of view, thus increasing the sheath capacitance, and

so, reduces $Z_{sh}$. This reduced sheath impedance thereby reduces the necessary value of $Z_L$. However, extra electrodes add to the overall dimensions and complexity of the probe. The question also arises as to what extend the measurement is *local* if large rf collection areas are implemented.

Reference electrodes are also used as indicators of distortion caused by drawing probe current from the plasma. In electron saturation, the current may be high enough that electron density in the vicinity of the probe becomes depleted. This causes a reduced electron saturation and also may distort the plasma potential, pushing it higher than it normally would be. This effect can be observed by simultaneous monitoring of the floating potential. If a change is observed, this can be then taken in to account in the analysis[6].

Rf compensation techniques have been shown to improve the Langmuir probe traces in some rf plasmas [5, 26], however, as the amplitude of oscillation increases, the requirements for sufficient compensation become extremely difficult to achieve in practice, and so, even compensated probes may suffer from distortion [25]. Part of the difficulty is that usually, in order to determine if a probe is properly compensated or not, it must be compared with another probe. Obviously, unless at least one of them is perfectly compensated, then the true measurement may not be known.

Another popular method is to use a 'driven' probe, in which the probe is driven with an out of phase oscillation at the same amplitude as the plasma oscillation. In this way, the effective oscillations can be made to cancel each other out at the tip [28, 29]. This is quite complicated however, and generally requires an accurate measurement of the plasma potential oscillation, such as that from a large area *loop probe* [24]. It may also be used without knowledge of the plasma oscillation by iteratively adjusting the amplitude and phase such that the measured floating potential reaches a maximum.

This indicates that time-averaging effects have been eliminated or at least reduced. However, the harmonics must also be compensated for, adding to the complexity of this system.

The work of Oksuz and Soberon [21], Crawford [30], Boschi and Magistrelli [31], Garscadden and Emeleus [32] show how oscillations cause distortion but also show how uncompensated probes can give reasonably accurate estimates of $T_e$ for moderate oscillation amplitudes. However, some of these references also require knowledge of $\tilde{\Phi}_{p_{rf}}$, which can be obtained in conjunction with a fully compensated probe, which defeats the purpose. Also, these techniques are usually limited to the higher energy tail of the distribution, where it is already obvious that the higher energy electrons will be less affected by the oscillations. So, in general, some form of compensation is required, even for small oscillations in plasma potential (relative to $T_e$) [33].

Additional sources of error which have not been mentioned are surface contamination, secondary emission, perturbation effects, reflection of electrons, external circuitry and oscillations, as given by Chen [4], Hershkowitz[34] and many others, [6–8, 20, 22, 28].

Finally, it should be noted that there are many other forms of invasive electrostatic diagnostics, such as, double Langmuir probes, emissive probes and resonance probes, each of which is generally more complicated than a single Langmuir probe and also suffer from many complications. These more complex diagnostics were essentially developed to alleviate the difficulties in measuring certain parameters with single Langmuir probes, but equally they have their own problems and limitations. In effect, these diagnostics demonstrate the potential beauty of Langmuirs original technique, a single piece of wire which can determine practically all of the important plasma parameters. Today, this is somewhat overcomplicated by the need for rf

compensation and incomplete theories for current collection, but as we shall see (sections 3.2 and 6), at least one of these issues may finally be overcome in a relatively simple way. ,

## 2.4   Summary

The main theoretical difficulties involved in matching the plasma parameters to the measured probe currents have been described. Many issues have been ignored, such as, the effects of multiple species, negative ions, magnetic fields and non-Maxwellian EEDF's, all of which are valid points of interest for todays industrial plasmas. However, as demonstrated, even in its simplest theoretical form, i.e Maxwellian low pressure, collisionless sheath etc, the Langmuir probe is anything but simple. The information contained in the I-V characteristic has also been explored, demonstrating the potential power of the technique and its usefulness which has ensured its continued use for over 80 years. It is the effect of oscillation which has been the main focus of this thesis. This effect on the measured current has been explained and the general difficulty and inadequacy of previous radio frequency compensation techniques have been described.

# CHAPTER 3

---

## Sheath Generated Harmonics

---

The effects of oscillations on the I-V characteristic were shown in chapter 2 In this chapter, we show exactly how and why time-averaged distortion occurs in uncompensated probes and how it is linked to the probe current harmonics generated by the sheath. It is understanding this relationship that allows the time-averaged distortion component to be separated from the total measured current, thus allowing undistorted I-V characteristics to be obtained without rf compensation.

## 3.1 Non-linear Sheath Impedance

The sheath formed around a probe can be simply modeled as a resistor, $R_{sh}$, in parallel with a capacitance, $C_{sh}$. The total impedance of the sheath, $Z_{sh}$, is then $(Xc_{sh}^{-1} + R_{sh}^{-1})^{-1}$, where $Xc_{sh}$ is the reactance of the sheath capac-

itance. The current collected will therefore consist of two components; direct current(real), and displacement current(imaginary). The resistive component can be understood simply as conventional resistance to the flow of charge carriers to the probe. The displacement current is caused by the oscillation of the charge carriers about the mean sheath width.

At large negative biases, all electrons are repelled while the ions are readily collected by the probe. This implies that the impedance depends on the sign of the carrier, similar to the behaviour of a diode. The sheath, formed between the plasma and probe tip, thus behaves as a non-linear impedance.

## 3.2 Harmonic generation and time-averaged distortion

An electrically floating surface will attain a dc potential (floating potential) when immersed in a plasma because the more mobile electrons initially arrive at that surface before the ions can respond. This floating potential depends on the ratio of the electron to ion mass. If an rf potential is applied to this surface, through a dc blocking capacitor, it has the effect of increasing the dc voltage across the sheath. This is a necessary requirement in order for the electron and ion fluxes to remain balanced and is known as the 'rf self bias' effect. Sturrock [35] was the first to propose an accurate mechanism for this effect. He showed that the non-linear properties of the sheath causes voltage rectification, which generates a time-averaged dc term, which then adds to the measured floating potential of an insulated probe.

In the absence of a blocking capacitor, the increased dc current due to this rf effect is known as *rectification current*. The relationship between rf amplitude and self-bias was also shown by Garscadden and Emeleus [32] RF

**Figure 3.1:** *Illustration of harmonic generation caused by non-linear sheath impedance The resultant waveform clearly has a non-zero time-averaged value.*

sheaths are thus wider than for dc plasmas.

The rectifying action and non-linear behaviour of capacitive sheaths has also been detailed by others [9, 36], but here we wish to examine these non-linear effects on Langmuir probe I-V characteristics.

Illustrated in figure (3.1), it is clear that an oscillation of the non-linear I-V characteristic must generate harmonics in the observed current. The effect of these harmonics is to create area-asymmetric current waveforms at each bias voltage, which therefore, must have non-zero time-averaged components, $\Delta I(V)$. In this case, the total time-averaged current measured by the probe is some unknown ratio of the desired dc current, $I_{DC_{eff}}$, plus $\Delta I$. This being the situation, it seems logical that there should be a fundamental link between $\Delta I$ and the harmonic amplitudes generated by the sheath.

Sloane and McGregor [37] were the first to propose a link between the sheath generated harmonics and an associated dc component. However, this aspect of their work appears to have been largely ignored in the literature, as practically all subsequent citations are in relation to their primary finding, which showed a seemingly more important link between the harmonics and the derivatives of the I-V characteristic. By applying a small oscillation to the probe and measuring the second harmonic as a function of dc bias, they showed that the second derivative of the I-V characteristic can be approximated, which can then be used to calculate accurate EEDF's via the Druyvestyn equation(3.1).

$$g_e(V) = \left( \frac{4}{eA} \sqrt{\frac{mE}{2e}} \right) \frac{d^2 I_e}{dV^2} \tag{3.1}$$

This method for obtaining the EEDF is now known as the a.c. superimposed method and originally had the advantage that it avoids errors caused by numerical differentiation.

For this thesis, the original work of Sloane and McGregor was re-examined to further explore the link between the harmonic amplitudes and the generated dc components. We developed a new approach based on fitting an $n^{th}$ order power series.

### 3.2.1 Mathematical model

The I-V characteristic can be fitted by an $n^{th}$ order power series of the following form:

$$i(V) = A_0 + A_1 V + A_2 V^2 + A_3 V^3 + \ldots\ldots$$

$$= \sum_{n=1}^{\infty} (A_n V^n) \tag{3.2}$$

*where $A_n$ are the coefficients of the power series and $n$ is the order.*

The collected current, $i$, is a function of the voltage, V. If we introduce an oscillating voltage, $V_{rf}$, then the equation for the rf current *only* becomes that of equation 3.3.

$$i(V_{rf}) = A_0 + A_1 V_o \sin(\omega t) + A_2 (V_o \sin(\omega t))^2 + A_3 (V_o \sin(\omega t))^3 + \ldots\ldots \tag{3.3}$$

where $V_o$ is the amplitude of the voltage sine wave, $V_{rf}$.

Expanding equation 3.3 with the appropriate trigonometric identities gives,

$$i(V_{rf}) = A_0 + A_1 V_o \sin(\omega t) + \frac{1}{2} A_2 V_o^2 - \frac{1}{2} A_2 V_o^2 \cos(2\omega t) + \ldots\ldots \tag{3.4}$$

Equation 3.4 is of the form of a Fourier series, with sine, cosine and dc terms separated. For clarity, only up to the $2^{nd}$ order is shown. $A_o$ equals zero in this case, but as can be seen, there is also an extra dc component with 2nd order terms, $\frac{1}{2} A_2 V_o^2$, generated purely by the non-linearity. Comparing this

with the amplitude of the second harmonic term, $-\frac{1}{2}A_2V_o^2\cos(2\omega t)$, we see that the magnitudes are identical (only the signs are opposite). This trend is repeated as higher terms are examined.

Removing all frequency dependant terms leaves only the rf sheath-generated dc components on the right hand side of equation 3.5.

$$i_{ave}(V_{rf}) = \frac{1}{2\pi}\int_0^{2\pi} i(V_{rf})$$

$$= \frac{1}{2}A_2V_0^2 + \frac{3}{8}A_4V_o^4 + \frac{5}{16}A_6V_o^6 + \dots$$

(3.5)

The frequency dependant terms *only* are given by $i_{rf}(V_{rf}) = i(V_{rf}) - i_{ave}(V_{rf})$. Equation 3.6 shows $i_{A_{rf}}(V_{rf})$, the resultant amplitudes of $i_{rf}(V_{rf})$, from the expansion of equation 3.4. **Only even terms are shown here.**

$$i_{A_{rf}}(V_{rf}) = -\frac{1}{2}A_2V_0^2 - \frac{3}{8}A_4V_o^4 - \frac{5}{16}A_6V_o^6 - \dots \qquad (3.6)$$

The terms in equation 3.5 represent the dc components generated purely by the non-linearity of the sheath, and as such, the sum of these dc terms must equal $\Delta I(V)$, therefore,

$$\frac{1}{2\pi}\int_0^{2\pi} i(V_{rf}) = -i_{A_{rf}}(V_{rf})$$

$$= \Delta I$$

(3.7)

at each point in bias, i.e. $\Delta I(V)$.

Equations **1.5 - 1.7** show two important results:

**1)** The oscillation of the non-linear sheath generates additional dc components, equation 3.5 (which sum together producing the time averaged distortion, $\Delta I$).

**2)** The sum of the sheath-generated *even* harmonic terms are identical in magnitude, but opposite in sign, to those of the corresponding dc terms. In other words, the sum of the *even* harmonic amplitudes replicate the dc terms generated by the sheath. This allows access to dc information purely through rf measurements and crucially allows the distortion component to be separated from the total measured current.

We find that only the *even* orders produce dc terms This is due to the fact that *even* orders of sine or cosine do not average to zero, while *odd* orders do. The polynomial order is directly related to the harmonic number, i e. the 2nd order term is equivalent to the 2nd harmonic etc.

With the necessary information contained in the harmonics, the corrected dc characteristic can be easily recovered from the distorted (measured) characteristic, $I_{ave}(V)$, via equation 3.8,

$$I_{DC_{eff}}(V) = I_{ave}(V) - \Delta I(V) \tag{3.8}$$

Equation 3.9 shows that due to frequency mixing in the sheath, the second harmonic contains components from *all* other *even* harmonics.

$$f_{2_{amp}} = -\frac{1}{2}A_2V_0^2 - \frac{1}{2}A_4V_0^4 - \frac{15}{32}A_6V_0^6 + ....  \qquad (3.9)$$

where; $f_{2_{amp}}$ is the second harmonic amplitude.

As shown, the amplitude of the second harmonic is composed of $2^{nd}$, $4^{th}$ and $6^{th}$ order terms, i e. terms from all the even harmonics. The highest order term in $f_{2_{amp}}$ is always the order of the polynomial (6th order in this case).

Equations (3 10) and (3.11) show the terms for the $4^{th}$ harmonic amplitude, $f_{4_{amp}}$, and $6^{th}$ harmonic amplitude, $f_{6_{amp}}$, respectively.

$$f_{4_{amp}} = (\frac{1}{8}A_4V_0^4 - \frac{3}{16}A_6V_0^6 + ...)  \qquad (3.10)$$

$$f_{6_{amp}} = (-\frac{1}{32}A_6V_0^6 + ...)  \qquad (3.11)$$

The sum of equations 3.9, 3.10 and 3.11 is equal to that of equation 3.6, the absolute value of which closely approximates $\Delta I$.

Comparing equation 3.5 with that of 3.9, it is clear that the second harmonic alone gives a reasonable approximation of $\Delta I$. As the amplitudes of higher order *even* harmonics are included, finer details in $\Delta I$ are approximated more closely. Thus, experimentally, measuring only the $f_2$ amplitude as a function of bias would be sufficient to give a good estimate of $\Delta I(V)$, thus allowing reasonably accurate reconstruction of $I_{DC_{eff}}(V)$.

The work by Sloane and McGregor [37] shows effectively the same result using a Taylor series expansion, as opposed to the power series presented here. The Taylor expansion shows that the approximation, of $f_{2_{amp}}(V) =$

$\frac{d^2i}{dV^2}$, is only valid if the oscillation amplitude is small, such that, the higher order terms of $f_2$ can be neglected. However, for determining $\Delta I$, no such limit applies. In fact, using more terms, $f_4$, $f_6$ etc. yields more accurate agreement.

## 3.3 Non-Sinusoidal and Dual Frequency Oscillations

Up until this point, only the case of single frequency oscillations have been considered. In practice, due to non-ideal matching networks, the plasma potential oscillation (at $f_{dr}$) is generally non-sinusoidal. The second harmonic component in particular, may be relatively large. For symmetric capacitive discharges, the second harmonic can dominate the plasma oscillation [24]. These multi-frequency signals make the previous analysis much more complicated.

For the single frequency case, it is clear that *any* harmonic that appears in the measured signal must have been created by the sheath. For a non-sinusoidal input oscillation, this is not true. If the exact oscillation is unknown, as is generally the case, then it is difficult to know which harmonics originate from the oscillation and which are generated by the sheath. It is only the sheath generated components that are of interest for this analysis.

Using the same basic mathematical procedure as for single frequency inputs, the case of a dual frequency input was examined. If $V_{rf} = V_o sin(\omega t) + V_H sin(\omega 2t)$, then, due to frequency mixing in the sheath, the *even* harmonic amplitudes may have contributions from *odd* harmonic components. Thus, an *even* harmonic amplitude may now be composed of sine and cosine terms from *every* other harmonic, not just *even* harmonics as was shown for the case

of single frequency oscillation. For the dual frequency situation, the terms become very large even at low orders of the polynomial, however, it can be shown that taking *only* the *cosine* terms of the *even* harmonics, reproduces $\Delta I(V)$ accurately.

Equation 3.12 shows the extra dc terms generated in this dual-frequency case, where $V_{2rf} = V_o sin(\omega t) + V_H sin(\omega 2t)$,

$$\frac{1}{2\pi} \int_0^{2\pi} i(V_{2rf}) = \frac{1}{2}A_2 V_0^2 + \frac{1}{2}A_2 V_H^2 + \frac{3}{8}A_4 V_o^4 + \frac{3}{8}A_4 V_H^4 + \frac{3}{2}A_4 V_o^2 V_H^2 + \ldots\ldots$$

$$(3.12)$$

Equation (3.12) shows how each frequency (of the dual-frequency input) produces a similar response, while the last term in the equation shows how the two signals interact with each other in the sheath to produce a more complicated expression for $\Delta I$. Examining the full Fourier series (not just the sheath generated dc terms shown here), it becomes apparent that summing the amplitudes of the *cosine terms only*, of *even* harmonics, returns the exact expression for $\Delta I$ (as in equation (3.12)) This has been shown in the dual-frequency case up to the 6th order polynomial. This analysis is independent of the frequencies chosen and implies that the analysis should work for any arbitrary periodic input oscillation.

## 3.4 Summary

The non-linear behaviour of the sheath has been explained, demonstrating how harmonics are generated due to the oscillating action of the sheath in an rf plasma.

The original work of Sloane and McGregor has been re-examined, demon-

strating that the sum of the sheath-generated *even* harmonic amplitudes is equal to the sheath-generated dc components, at each point in bias. The fact that this dc component is actually the source of the time-averaged distortion to I-V characteristics has not been stated before in the literature. This fact was either ignored or simply overlooked in the intervening years. Thus, it appears that extracting the correct dc characteristic from the distorted one, using the harmonic information, is apparently a new idea.

The dual frequency case has also been investigated, with results indicating that corrected I-V characteristics can still be obtained without the need for rf compensation. This could be of significant importance for many industrial plasmas.

Having demonstrated mathematically that separating $\Delta I$ is possible, a circuit was designed to test this experimentally. A computer simulation was developed to investigate the expected output from the experiments, which enabled a deeper understanding of the technique, allowing new possibilities to be explored quickly and easily. This is discussed in the next chapter.

# CHAPTER 4

---

# Computer Simulation

---

A basic analytical computer model was written in MatLab to simulate phase dependant I-V characteristics of an arbitrary rf plasma. The density, electron temperature and plasma oscillation amplitude are variable. Phase-dependant I-V characteristics are generated over the input dc sweep range. This allows the rf currents to be examined at each bias voltage and harmonics obtained via FFT of the collected waveforms. For simplicity, frequency effects are ignored, as is the non-linear behaviour of the sheath capacitance. The effect of these simplifications will be discussed at the end of the chapter.

## 4.1   Design of Measurement Circuit

In order to experimentally measure the harmonics and record the rf waveform information a circuit was designed, as shown in figure (4.1). This is the circuit
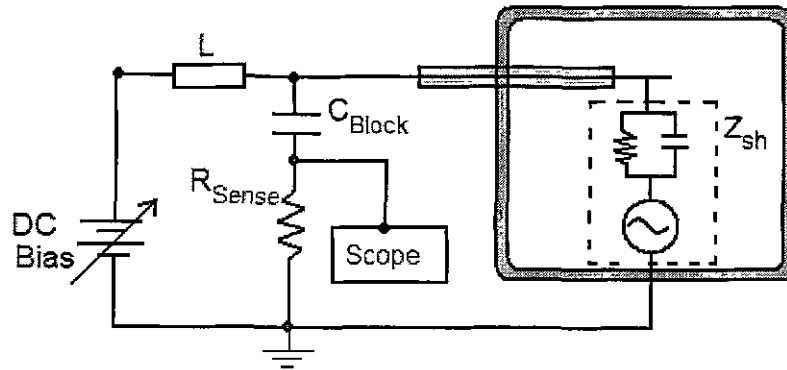
**Figure 4.1:** *Diagram of the measurement circuit*

simulated by the Matlab model.

With a "standard" Langmuir probe circuit, only the dc current component is desired, so no effort is made to observe the rf components. In this case however, the rf currents are to be measured as a function of dc bias voltage.

As can be seen in figure (4.1), the circuit is not much different to a regular Langmuir probe circuit. The major change is that an rf measurement branch has been included. This is made up of a blocking capacitor and resistor in series. An rf inductor is also included on the dc line so as to prevent rf currents affecting the dc supply or rf measurement accuracy. The rf measurement resistor, $R_{sense}$, is in series with the dc blocking capacitor, thus, no dc current can be measured across $R_{sense}$. The rf current at the tip (caused by the plasma potential oscillation) will therefore see a relatively easy path to ground through the low impedance capacitance and $R_{sense}$, which is generally 50 Ohms. Even if the inductor is not tuned very accurately to the required frequency, it will still have a much higher impedance than 50 ohms, thus a very large percentage of the rf current arriving at the tip will flow

48

exclusively through the rf measurement branch and induce a proportionate voltage drop across $R_{sense}$. The value for $R_{sense}$ was originally chosen to be $50\Omega$ as the probe itself is constructed of $50\Omega$ semi-rigid coaxial cable (see figure (5.2)) This impedance matching ensures maximum transfer of current, from tip to $R_{sense}$, by minimising reflections. This allows the probe to be modeled as a transmission line to observe how changes in impedance may affect the measured signals. In this case, the source impedance is that of the sheath, while $R_{sense}$ acts as the load termination. The results indicate that in this configuration the probe should act like a near perfect transmission line.

This circuit is dc biased while the rf current is measured across $R_{sense}$. In this way, an 'RF I-V characteristic' can be generated. To understand what this would look like and exactly how useful information can be extracted from it, the simulation was used.

## 4.2 Simulation Basics

Essentially, equations 2.1 - 2.3 are used to calculate ion and electron currents as a function of the dc bias voltage, thus giving $I_{DC}(V)$. The total time-dependant current (rf plus dc current), $\tilde{I}_{total}(V, \tilde{V}_{sh}, t)$, is calculated by introducing a time-varying plasma potential oscillation. At each time step the current is calculated, thus, for each bias voltage, a time-dependant waveform is created. The resultant fast Fourier transform (FFT) of each waveform is then calculated. Time-dependant I-V characteristics produced by this simulation have already been shown in figure (2.2).

Frequency effects on the oscillating I-V characteristics are not taken into account, except that the value of $X_{c_{sh}}$, the capacitive reactance of the sheath,

does change with frequency. $X_{c_{sh}}$ is calculated from the sheath width using the cylindrical capacitance equation. Therefore, the capacitance of the sheath is not modeled as a non-linear component, and so, the I-V characteristic does not change shape as a function of phase, no matter what the frequency. The sheath resistance, $R_{sh}$ is given by $(\tilde{V}_{sh}/\tilde{I}_{total})$, assuming the circuit resistance, $R_{circuit} << R_{sh}$. The value of $X_{c_{sh}}$ is added in parallel to $R_{sh}$ to simulate the resultant total sheath impedance, $Z_{sh}$.

The ion currents may be included or removed from $\tilde{I}_{rf}(V, \tilde{V}_{sh}, \phi)$ for better comparison with low and high frequency experimental results. However, the simulation shows that the inclusion or removal of ion current does not change any of the results significantly, as the electron current is by far the dominate one

## 4.3 Simulated Data

### 4.3.1 ΔI Measurements

Because frequency effects are not considered in this simulation, $I(V, 0, 0)$ $\equiv I_{DC}(V)$. In practice however, due to changes in sheath impedance with frequency (due largely to the non-linear sheath capacitance), $I_{DC}(V)$ is modified, such that, $I_{DC}(V) \neq I(V, 0, 0)$. Thus, in the experiment, $I(V, 0, 0) = I_{DC_{eff}}(V)$

Figure(2.3) clearly shows that $I_{ave}(V)$ is distorted by the time-averaging effect but to observe this distortion directly, as a function of bias voltage, $I_{ave}(V)$ - $I_{DC}(V)$ is plotted in figure (4.2).

According to the mathematical analysis of **3.2.1**, the sum of the *even* harmonic amplitudes should equal ΔI. The harmonics are measured by performing a FFT on the generated waveform data, at each point in bias voltage.
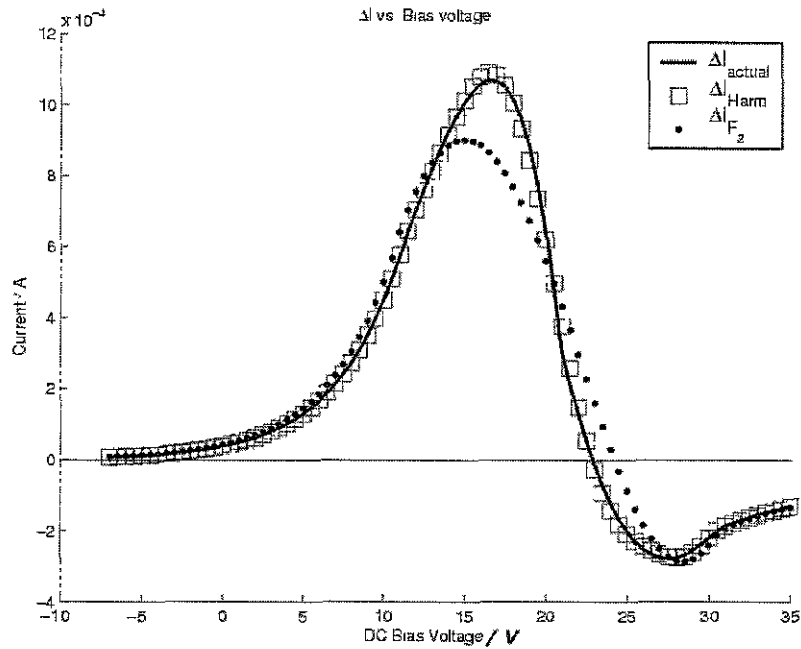
**Figure 4.2:** $\Delta I$ as a function of bias voltage. The solid line is the actual $\Delta I$. $\Delta I_{Harm}$ represents the sum of the first 4 even harmonic amplitudes (squares) and $\Delta I_{f_2}$ is the second harmonic amplitude only (dots), as a function of bias.

A comparison of the actual distortion, $\Delta I(V)$, and the reconstructed distortion, $\Delta I_{Harm}(V)$, is shown in figure (4.2). Also shown is $\Delta I_{f2}(V)$, which is simply the amplitude of the measured second harmonic, $f_2$ as a function of bias. The fact that $f_2(V)$ only is a reasonable approximation of $\Delta I$ is in good agreement with the mathematical analysis. The simulation also shows that the number of harmonics necessary for a close fit to $\Delta I$ is generally small, but if the dc characteristic has a sharper 'knee', higher order harmonics must also be summed. Again, this is in agreement with the mathematical model, which shows that higher order polynomials are required to fit a 'sharper' characteristic, thus the harmonic content is greater.

Figure(4.3) demonstrates that the dc trace is almost perfectly recon-
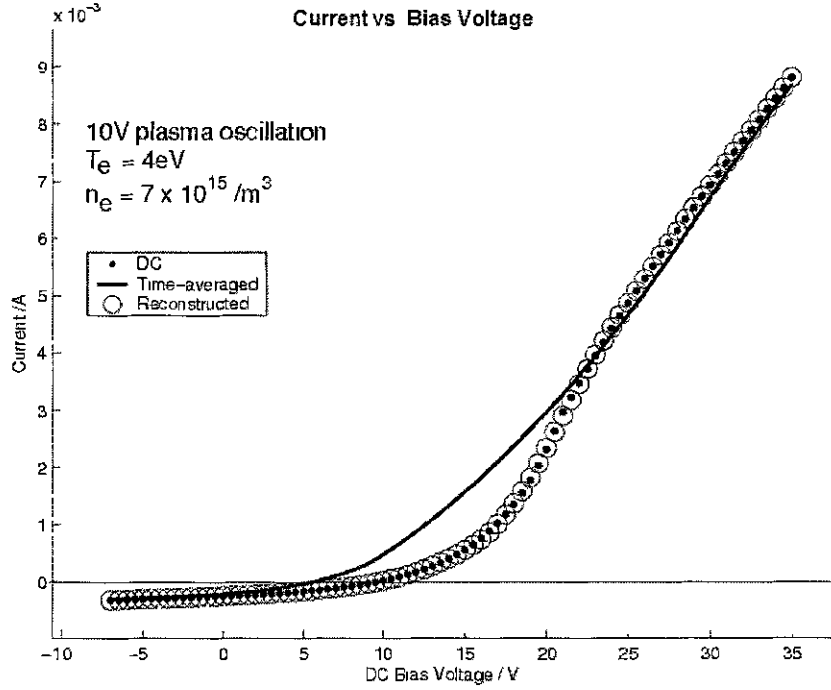
**Figure 4.3:** *Reconstructed DC characteristic: The dots represent the actual DC trace, while the circles are the 'corrected' time averaged values, i.e. $I_{ave}$ - $\Delta I_{Harm}$. The time-averaged (distorted) trace is also shown for comparison.*

structed from $I_{ave}(V)$ - $\Delta I_{Harm}(V)$.

The simulation also shows that the oscillation magnitude can be found using the $\Delta I$ versus bias voltage curve. It is found that the voltage difference between the zero crossing point and the peak of $\Delta I(V)$, gives the oscillation magnitude. For very small oscillations, $f_2 \approx (d^2I/dV^2)$, in which case, the peak and zero-crossing points should be at the same potential.

The fact that the $\Delta I$ curve changes sign (polarity), as a function of bias voltage, presents some difficulties when reconstructing $I_{DC}(V)$ from the harmonics. If an unknown phase-shift occurs in the measured waveforms, the absolute harmonic amplitudes must be used ($\sqrt{(Real)^2 + (imaginary)^2}$), be-
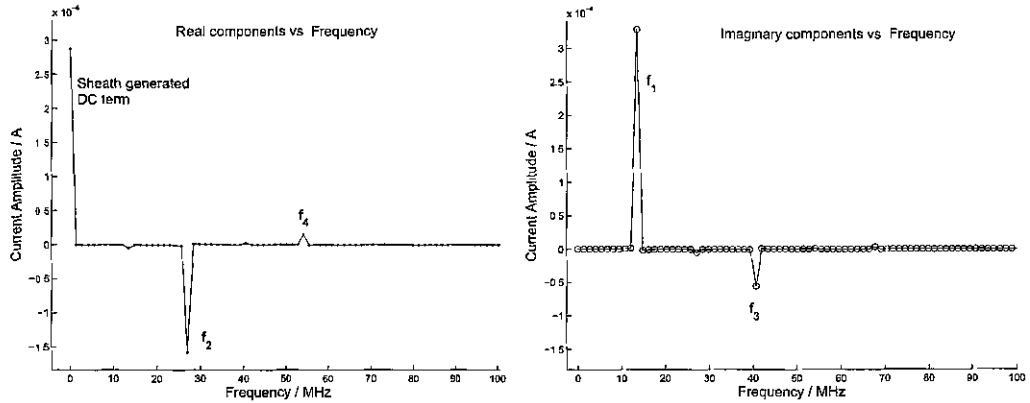
**Figure 4.4:** *Simulated FFT of a current waveform at one particular bias voltage. (Left) The real components only. (Right) The imaginary components only. These show that the* even *harmonics are entirely* real, *while* odd *harmonics are* imaginary.

cause as equation (4.1) shows, a change in phase causes a change in the ratio of real to imaginary components. If the absolute values are used, then each harmonic amplitude will appear entirely positive as a function of bias voltage. This becomes a problem when the *even* harmonics are summed, resulting in an incorrect $\Delta I(V)$ curve.

$$\phi = \tan^{-1}\left(Imaginary/Real\right) \qquad (4.1)$$

For a pure sinusoidal input oscillation with no phase-shifts incurred during measurement, it is not necessary to use the absolute values, as all the *even* harmonics are entirely *real*, while the *odd* harmonics are entirely *imaginary*. This is illustrated in the FFT of figure(4.4).

In this case, simply using the sum of the *real* components of the FFT maintains the polarity information, thus allowing the exact $\Delta I(V)$ curve to be recovered.

Although changing phase of the input oscillation from sine to cosine may

seem like an arbitrary difference, it actually causes an incorrect summation of the *even* harmonics. This is due to the fact that cosine inputs produce only positive valued harmonic components. This is easily shown by substituting a cosine oscillation into the mathematical analysis of section (3.2.1). The magnitudes may be correct, but the polarities are not, thus, only sine oscillations (starting at zero amplitude at t $= 0$) can reproduce $\Delta$I straightforwardly from the sum of the harmonics. In general, some phase-shifts will always be incurred in the experiment, so it is best to use the absolute values.

The absolute value of $f_2$(V) approximates $\Delta$I(V), but because $abs(f_2(V))$ is entirely positive an inflection point occurs, thus marking the point in bias where $\Delta$I(V) goes negative. To get a more accurate reconstruction of $\Delta$I(V) requires the summation of more *even* harmonics of the correct polarity. One possible way to obtain this polarity information is described by equation 4 2

$$abs(f_x)_{Corrected} = abs(f_x) \times \left( real(f_x)/real(f_x)^2 \right) \qquad (4.2)$$

where x is the harmonic number. The term in brackets is only calculated at one point in bias to determine an initial polarity. The imaginary components could also be used

$Real(f_4)$ and abs($f_4$) are illustrated in figure(4.5). To determine the appropriate polarity from abs($f_4$), the *real* value of $f_4$ is determined at one bias voltage below the first inflection point. Depending on the polarity of this value, the term in brackets in equation 4.2 is either 1 or -1. This gives the appropriate orientation of $abs(f_4)$, which is then modified positive or negative at the inflection points as required.

This has been proven to work well in the simulation but is sometimes prone to error if the initial reference point is noisy as this can cause false polarity readings. Errors can generally be avoided by choosing a bias point
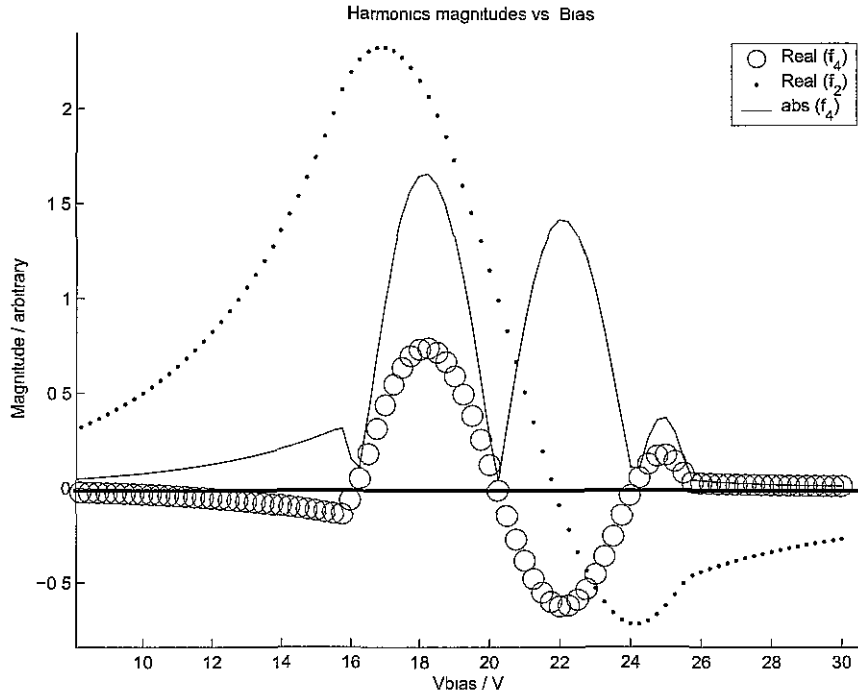
**Figure 4.5:** *Fourth harmonic versus bias voltage. The absolute and real values are shown. The inflection points can clearly be seen. $f_2$ is also plotted for comparison.*

m the exponential region, where the signal to noise ratio is sufficiently large not to cause false polarity readings.

## 4.3.2 RF Measurements

Figure (4.6) shows the rf current waveforms output from the model as a function of bias voltage, $\tilde{I}_{rf}(V, \tilde{V}_{sh}(t))$. This is for an input oscillation of 5V amplitude. Figure (4.7) is constructed by transposing the waveform data of figure (4.6) and plotting against bias voltage to obtain $\tilde{I}_{rf}(V, \tilde{V}_{sh}, \phi)$. The resultant graph, called an 'RF I-V characteristic', is plotted over one full period of oscillation, thus each line represents the rf current magnitude at a different point in phase, as a function of bias voltage.
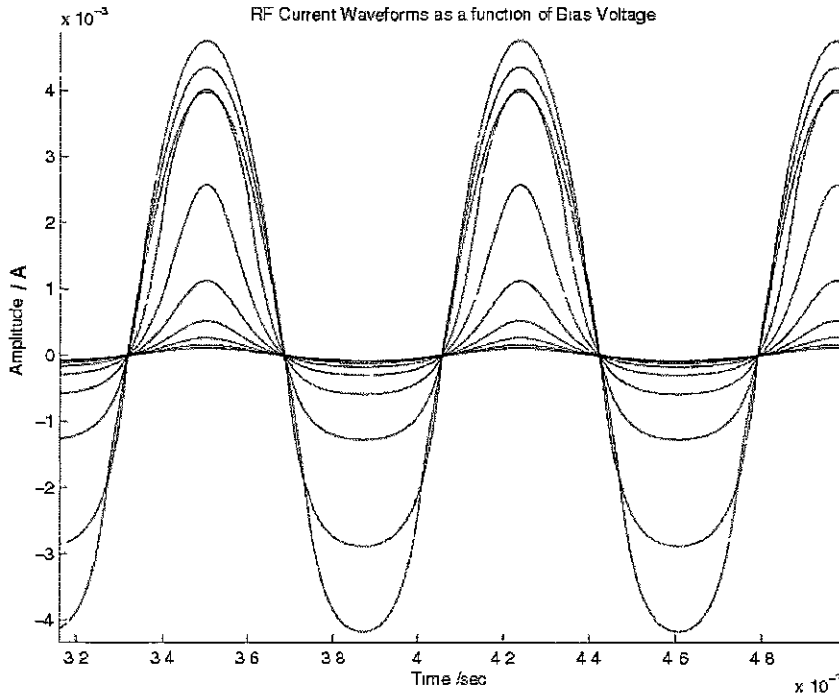
**Figure 4.6:** *Simulated RF current waveforms collected as a function of dc bias voltage*

The blocking capacitor in the circuit prevents *all* dc signals from being measured at $R_{sense}$, so the expected appearance of the experimentally measured rf I-V characteristics is that of figure (4.7 (Left)). In figure (4.7 (Right)), $\Delta I$ has been added back.

The simulation shows that this *modified rf I-V characteristic* can be used to determine the magnitude of the plasma oscillation. It can be shown that the the voltage difference between the the positive and negative peaks of the modified rf I-V characteristic reveals the plasma oscillation magnitude. For the data in figure (4.7), the oscillation amplitude was 10 $V_{pk-pk}$. For dual frequency inputs the total maximum magnitude of the oscillation is given, not amplitude, as in the single frequency case.
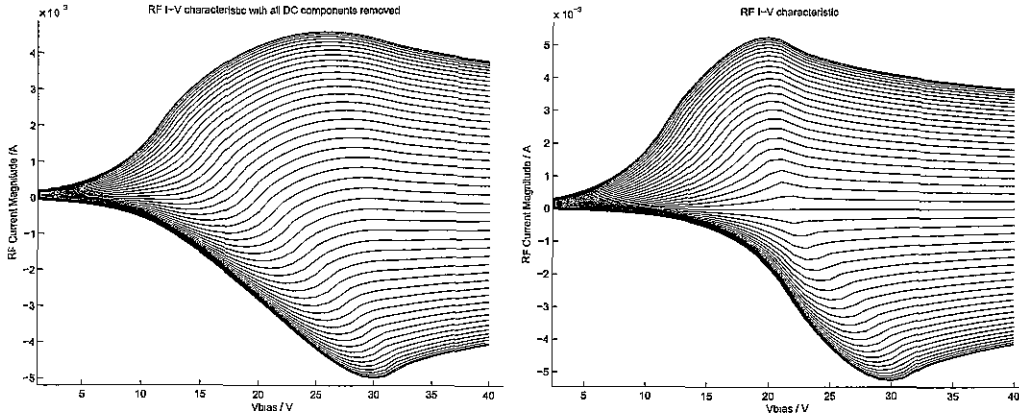
**Figure 4.7:** *RF current versus bias, as a function of phase. (Left): RF I-V characteristic with ΔI removed.(Right): Modified RF I-V characteristic, i.e. the rf current + ΔI as a function of dc bias voltage.*

An important point to note is that a phase-shift will occur in the measured current waveforms due to the change in sheath impedance with bias voltage (Eqn.(4.9)). As bias is varied, the measured waveforms will change phase relative to the time varying plasma potential. This distorts the recovered rf I-V information, thus phase-shifts must be removed. Removal of phase shifts from the experimental data is explained in more detail in (5.2.5).

## 4.3.3 Reconstructing Phase-Dependant Characteristics

Using the simulation, a simple method for reconstructing the correct phase-dependant I-V characteristics was determined. It can be shown that only the distorted (time-averaged) characteristic and the rf current measurements are needed. This is explained as follows:

The rf I-V trace effectively shows the magnitude of the current oscillation on the dc I-V characteristic. These oscillating currents generate time-averaged dc components, $\Delta I(V)$. If these dc components are removed by

the capacitor, then $\tilde{I}_{RF_{meas}}(V, \tilde{V}_{sh}, \phi)$ is the phase-dependant rf current measured at $R_{sense}$ for each bias voltage. The time-average of $\tilde{I}_{RF_{meas}}(V, \tilde{V}_{sh}, \phi)$ is therefore equal to zero.

The rf currents oscillate about some dc value, so,

$$I_{DC}(V) + \Delta I(V) + \tilde{I}_{RF_{meas}}(V, \tilde{V}_{sh}, \phi) = \tilde{I}_{total}(V, \tilde{V}_{sh}, \phi) \qquad (4.3)$$

Equation 4 3 determines the total current at any point in phase of the plasma potential oscillation. The resultant time-average over one full period of the phase-dependant characteristics must equal the distorted trace, $I_{ave}(V)$.

Figure (4.7 (Right)) shows that, at t = 0,

$$\Delta I(V) + \tilde{I}_{RF_{meas}}(V, \tilde{V}_{sh}, \phi) = 0 \qquad (4.4)$$

Hence,

$$\tilde{I}_{total}(V, 0, 0) = I_{DC}(V) \qquad (4.5)$$

Experimentally, $I_{DC}(V)$ cannot be obtained directly with an uncompensated probe, however, as shown, it can be calculated from $I_{ave}(V)$ - $\Delta I(V)$, thus

$$\tilde{I}_{total}(V, \tilde{V}_{sh}, \phi) = (I_{ave}(V) - \Delta I(V)) + \tilde{I}_{RF_{meas}}(V, \tilde{V}_{sh}, \phi) + \Delta I(V)$$
$$\Rightarrow \tilde{I}_{total}(V, \tilde{V}_{sh}, \phi) = I_{ave}(V) + \tilde{I}_{RF_{meas}}(V, \tilde{V}_{sh}, \phi) \qquad (4.6)$$

This implies that simply adding the measured characteristic, $I_{ave}(V)$, to the measured rf I-V characteristic, $\tilde{I}_{RF_{meas}}(V, \tilde{V}_{sh}, \phi)$, returns exactly the correct phase dependant I-V characteristics. From this the dc trace (at t = 0) and also the time-varying plasma potential can be obtained.
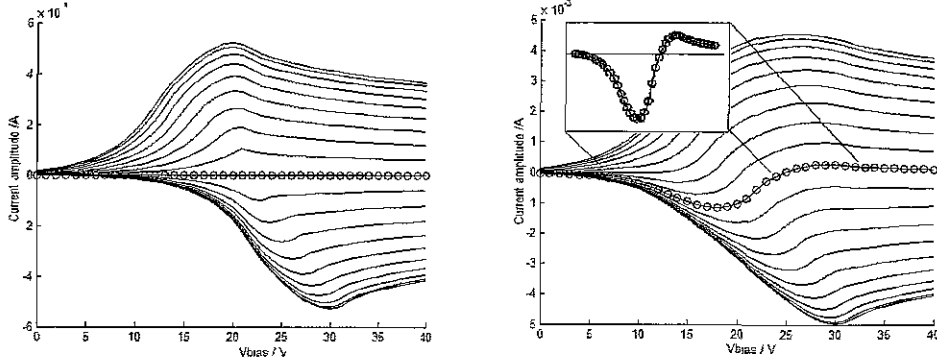
**Figure 4.8:** *Simulated data: (Left)Modified RF I-V characteristic, i.e. the rf current + ΔI, versus bias as a function of phase. The (t=0) trace is highlighted by circles. (Right) RF I-V characteristic with ΔI(V) removed. The (t=0) trace is also highlighted and expanded. This equals (-1)ΔI(V) exactly.*

Again, the simulation was used to verify this, and indeed, was found to be correct. This also leads to the interesting fact that at t = 0, $\tilde{I}_{RF_{meas}}(V, 0, 0)$ = - ΔI(V). Thus, instead of measuring the harmonics, and all the difficulties that presents, ΔI(V) can be obtained simply from the $t = 0$ trace of the rf I-V characteristic. This is shown in figure 4.8(right).

For these simulations, the shape of the characteristics are not phase-dependant, as frequency effects are not accounted for (non-linear sheath capacitance is ignored). In practice, this is not the case and predicting the exact behaviour is very difficult. Traditionally, experimental comparison has been limited by the fact that there is no simple diagnostic method available to measure phase-dependant I-V characteristics at high frequencies. Sweeping the entire bias range as quickly as possible and repeat within a fraction of the a.c. cycle is generally not feasible, as this requires the ion sheath to respond on the same time scale. Due to a combination of ion response time and circuit capacitance most systems are limited to $<< \omega_{ion}$.

With the new technique presented in this thesis however, the dc scan

**59**

rate can be as slow as required, thus giving the ion sheath plenty of time to adjust between subsequent measurements. The a.c. information is acquired separately, so this method avoids the above issues with previous methods. Possible frequency effects are explored in section 4.6.

### 4.3.4 Measuring the phase-dependant plasma potential

Assuming the phase-dependant I-V characteristics are measured, the time-dependant plasma oscillation, $\tilde{\Phi}_p(t)$, can be reconstructed. At

$$
\begin{aligned}
\tilde{I}''_{total}(V, \tilde{V}_{sh}, \phi) &= 0 \\
\tilde{\Phi}_p(t) &= V
\end{aligned}
\tag{4.7}
$$

This was verified with the simulation for single and dual frequency input oscillations. A reconstructed non-sinusoidal oscillation waveform is shown in figure(4.9). This shows that the reconstruction is near perfect. For accurate reconstruction of $\tilde{\Phi}_p(t)$ from $\tilde{I}_{total}(V, \tilde{V}_{sh}, \phi)$, the simulation shows that $\Delta_{V_{Bias}} \ll \tilde{\Phi}_{p_{rf}}$, where $\Delta_{V_{Bias}}$ is the bias voltage increment. If $I_{tot}''(V, \tilde{V}_{sh}, \phi)$ is too noisy, the maximum peaks of $I_{tot}'(V, \tilde{V}_{sh}, \phi)$ can also be used.

### 4.3.5 Measuring the complex sheath impedance

For the situation shown in figure(4.10), the voltage divider equation gives

$$
V_{meas} = \tilde{\Phi}_{rf}\left( R_{sense}/(Z_{sh} + R_{sense}) \right)
\tag{4.8}
$$

where $\tilde{\Phi}_{rf}$ is the oscillating component of the total plasma potential, $\tilde{\Phi}_p$. $V_{meas}$ is the measured voltage across $R_{sense}$.

Voltage magnitude vs. Time
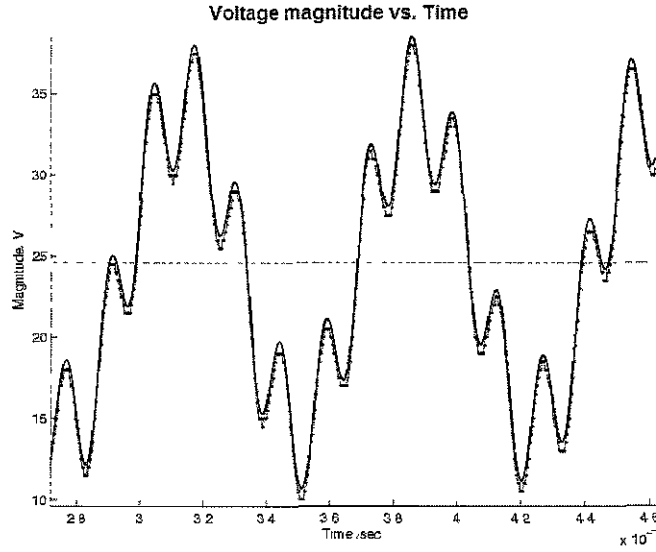


**Figure 4.9:** *Simulated reconstruction of a non-sinusoidal plasma oscillation from the phase-dependant I-V characteristics. The dc plasma potential is shown to be about 24 V. The input oscillation was a superposition of 13.56 MHz and 73 MHz signals, of 10 V and 4 V amplitude, respectively. The solid line is the actual oscillation input, while the dots are the reconstructed points.*

Using the method previously described to accurately measure the plasma potential as a function of phase, all parameters in equation(4.8) are known and a solution for the complex sheath impedance can be obtained.

Before we can accurately determine the sheath impedance, the phase shift induced by the series combination of sheath capacitive reactance, $X_{c_{sh}}$, and $R_{sense}$ must be taken into account. The phase shift in a series RC network is given by

$$\phi_m = \tan^{-}1(-X_{c_{sh}}/R_{sense}) \tag{4.9}$$

From this, it is clear that the phase shift will be very close to 90 degrees

61
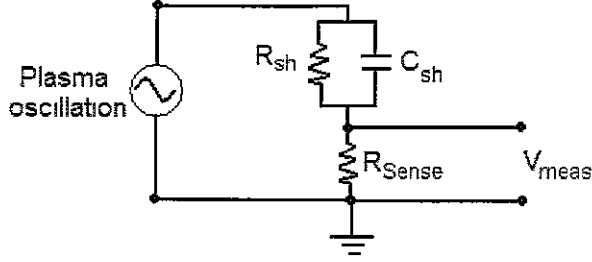
**Figure 4.10:** *Equivalent circuit for oscillating current. The blocking capacitor impedance is not shown as it is negligible compared with $R_{sense}$.*

when $X_{c_{sh}} >> R_{sense}$. In ion saturation this condition is satisfied, so for large negative bias voltages, the measured waveforms at $R_{sense}$ will be 90 degrees out of phase with respect to the plasma oscillation This gives us an initial phase reference for $\tilde{\Phi}_{p_{rf}}$.

As the bias voltage approaches the plasma potential, $X_{c_{sh}}$ diminishes and the phase changes. At the plasma potential, when the sheath collapses completely, the impedance is purely resistive. The phase shift should therefore be 90 degrees with respect to its original value in ion saturation. Because $R_{sense}$ is non-reactive, the current flowing through it is in phase with the voltage it develops so the measured signal at $V = \tilde{\Phi}_p$ is in phase with the plasma potential.

In order to solve equation (4.9) for the complex form of $Z_{sh}$, the measured voltage at $R_{sense}$ must also be in complex form. This is constructed using

$$V_{meas}{}^* = \left(V_{m_{amp}} * Cos(\phi_m)\right) + \left(V_{m_{amp}} * jSin(\phi_m)\right) \qquad (4.10)$$

where; $V_{meas}{}^*$ is the complex form of the measured voltage at $R_{sense}$, $V_{m_{amp}}$ is the measured amplitude at a particular frequency and $\phi_m$ is the phase shift between the measured signals and $\tilde{\Phi}_{p_{rf}}$

To get an undistorted amplitude value for each frequency, the absolute values of the FFT's are used to obtain $V_{m_{amp}}$. Solving equation(4.8) using the complex form of $V_{meas}$ from equation(4.10), the resultant complex form of the sheath impedance can be separated into its real and imaginary components.

Assuming $R_{sh}$ is purely real and $X_{c_{sh}}$ is purely imaginary, it can be shown that

$$R_{sh} = (Z_{sh_{real}}^{2} + Z_{sh_{imag}}^{2})/Z_{real} \tag{4.11}$$

and

$$X_{c_{sh}} = (Z_{sh_{real}}^{2} + Z_{sh_{imag}}^{2})/Z_{imag} \tag{4.12}$$

where;

$Z_{sh_{real}}$ = real component of $Z_{sh}$

$Z_{sh_{imag}}$ = imaginary component of $Z_{sh}$

Therefore, this allows us to not only accurately measure the sheath impedance, but also to investigate the individual components. This may be important for investigating the sheath behaviour in more detail or for probe tips which become coated with an insulting layer during operation.

## 4.4 The $R_{sense}$ Loading Effect

The simulation shows that under certain conditions, the $50\Omega$ resistor used in the measurement circuit may actually cause a significant effect on the resultant harmonics. This *loading effect* depends on the ratio of $R_{sense}$ to the rf impedance of the sheath, $Z_{RF}$. As the probe tip potential approaches
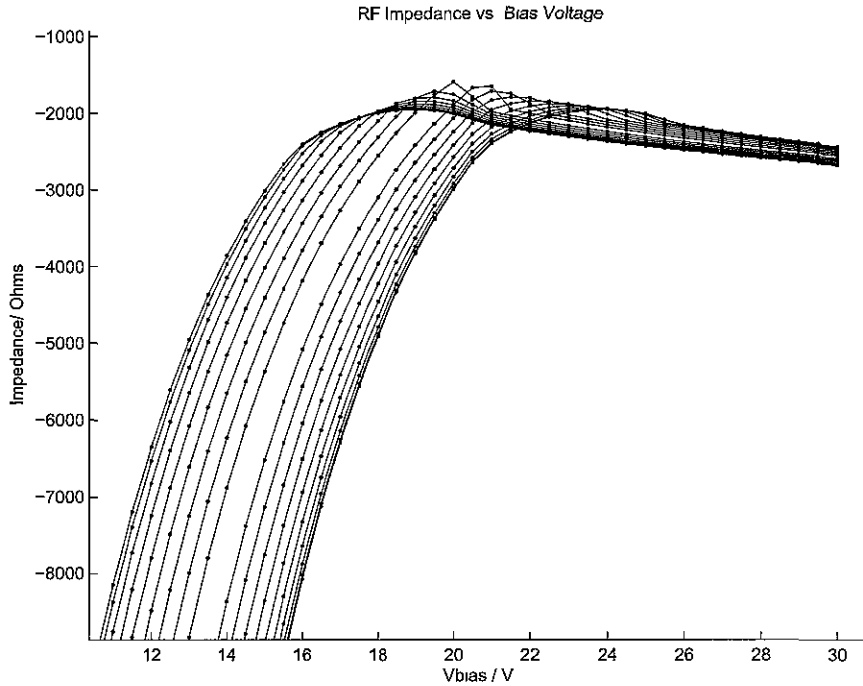
**Figure 4.11:** *RF Impedance as a function of bias voltage and phase;* $Z_{RF}(V,\phi)$ $= (\tilde{\Phi}_{p_{rf}}(\phi) \ / \ \tilde{I}_{RF}(V,\phi))$

the plasma potential, $R_{sense}$ can become a significant fraction of $Z_{RF}$ (particularly at high density, where the minimum in $Z_{RF}$ is relatively low). Effectively, the resistor limits the current and leads to a 'linearisation' effect. This causes a reduction in the amplitude and number of observed harmonics. Essentially, it causes distortion of the reconstructed $\Delta I(V)$, as the harmonics are disturbed by the process of measurement.

Figure(4.11) shows a low density case $(7 \times 10^{15} m^{-3})$, with $R_{sense} = 50\Omega$. The minimum value of the rf impedance is about $1600\Omega$, so $R_{sense}$ will have a negligible effect here. At $2 \times 10^{17} m^{-3}$ the minimum reduces to about $50\Omega$, so clearly at high density this effect may become a problem.

A modified circuit, which uses a current transformer sensor instead of a resistance, was designed to eliminate or at least reduce this effect in the

**64**

experiment. This is explained further in **Chapter 5 (5.2.3)**.

## 4.5 Dual Frequency Simulations

When both driven frequencies, $f_o$ and $f_H$, are sine waves with zero phase, the FFT gives cosine terms represented by the *real* components, while the *imaginary* components represent the sine terms. As explained in 3.3, for a dual frequency input oscillation, summing only the cosine terms of the *even* harmonics reconstructs $\Delta I(V)$ accurately. Therefore, in this dual frequency case, the *real* amplitudes of the *even* harmonics are used to obtain $\Delta I(V)$.

Figure(4.12) shows a dual frequency $\Delta I(V)$ curve and also curves reconstructed from the harmonic amplitudes. $f_{o2}(V)$ alone gives a reasonably accurate reconstruction of $\Delta I(V)$, where $f_{o2}$ is the sheath-generated second harmonic component of the first frequency, $f_o$. It is observed however, that the approximation $f_{o2}(V) \approx \Delta I(V)$ becomes less accurate as the ratio of $V_H/V_o$ increases. The *even* terms of $f_H$ must therefore also be included.

Figure(4.12) essentially illustrates the level of error that would be imposed on the reconstructed $\Delta I(V)$ by a slightly non-sinusoidal plasma potential oscillation (fundamental plus 20% harmonic amplitude). This is a likely situation in many single-frequency plasma systems with non-ideal power sources. Thus, if the ratio of the amplitudes, $V_H/V_o$, is small, using only the *even* harmonics of the main frequency component gives a reasonably accurate reconstruction of $\Delta I(V)$.

This dual frequency analysis becomes more complicated if there is a phase-shift between the two frequencies. Effectively, the *real* values of the FFT are *contaminated* by the phase shift, i.e. a change in phase causes a change in the ratio of real to imaginary components, thus making it im-
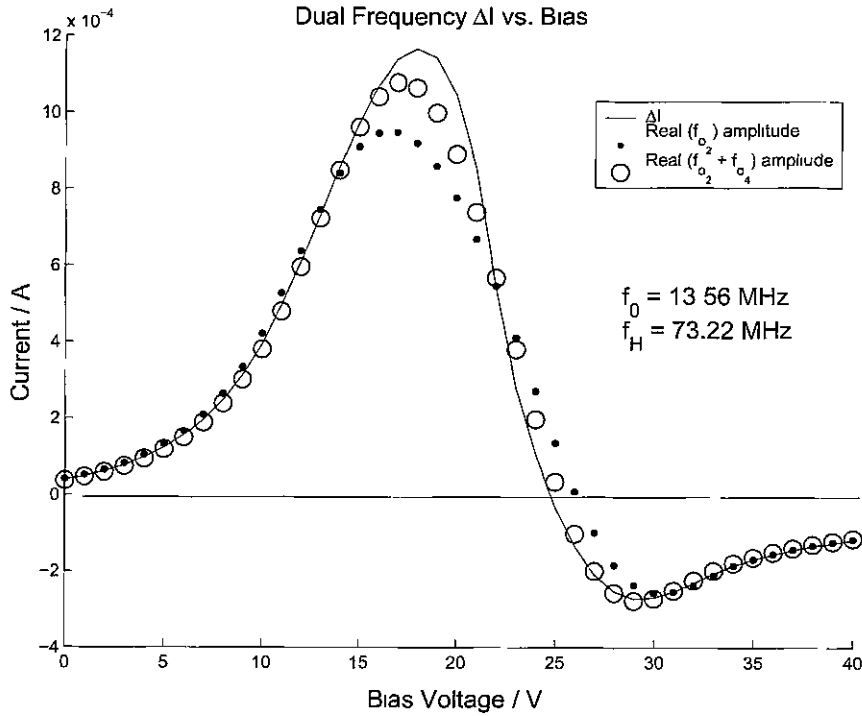
**Figure 4.12:** *Dual frequency $\Delta I$ and the reconstructed $\Delta I$ from $f_{o_2}$ only and $f_{o_2} + f_{o_4}$. The amplitudes of the two frequency inputs were $V_o = 10$ V and $V_H = 2$ V. In this example, only the sheath-generated frequency components of $f_o$ are used in the reconstructed $\Delta I$ curves.*

possible to determine which parts of the real components are due *only* to sheath-generated harmonic terms. So again phase-shifts have proven to increase the complexity of the analysis.

## 4.6 Frequency effects on $\Delta$I

As the frequency increases, $X_{c_{sh}}$ becomes more significant and the total sheath impedance departs from the basic dc model[9], due in part to the nonlinear sheath capacitance. Thus, $\Delta$I(V) changes as a function of frequency because the shape of the characteristic changes. This should have no effect
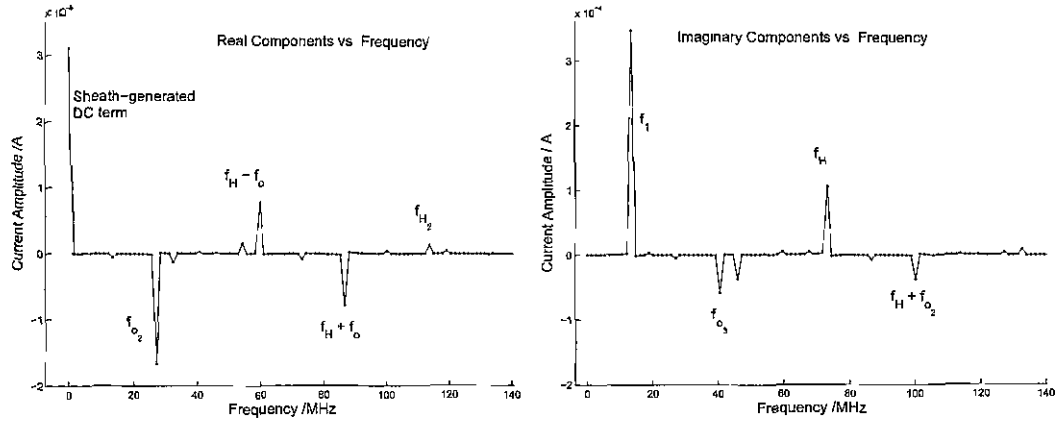
**Figure 4.13:** *Dual frequency FFT at one particular bias voltage. This illustrates the complexity caused by multiple frequency interactions: (Left)Real components only (Right) Imaginary components only.*

on the validity of this method however, as the amplitudes of the harmonics also change in a corresponding way. To a certain extent this has already been shown in the mathematical model by not defining the coefficients of the polynomial. However, what happens if the characteristic changes shape as a function of phase?

The literature shows that there is an assumed upper frequency limit $(f \ll f_{ion})$ when using the superimposed a c. EEDF method, described by many authors[38–40]. It appears to be assumed that the method will not work at higher frequencies, but is difficult to find references that actually explain the reasoning behind this.

Presumably, low frequencies were used to ensure that the characteristic remains essentially resistive, and so, does not change shape appreciably as a function of phase. However, in a recent paper by Chen(2006) [33], an equation for the time-dependant sheath capacitance is given for planar geometry. Unfortunately, extension to the transition region of cylindrical probes is only possible through numerical integration. The sheath capacitance as a func-

tion of bias is given for the electron saturation region of a cylindrical probe (calculated from OML theory). These results are only valid for low frequency cases where the ions can respond, but even so, it is shown that the sheath capacitance, in particular, will cause many harmonics to be generated, at least for planar probes. For the cylindrical case, the harmonics will be less, due to the continuous nature of the curve as the electron saturation region is encountered. These results seem to indicate that even at low frequencies, the shape of the characteristic must change as a function of phase, which is *not* the case investigated in the mathematical model given in section (3.2), or that of papers regarding the a.c. method for EEDF measurement.

The question of whether or not our analysis is fundamentally valid at higher frequencies is not easy to answer, but some of the issues are examined in the next sub-section, where the work on resonance probes offers further insight into the behaviour of $\Delta$I as a function of frequency

## 4.6.1 Resonance Probes

Much of the work on resonance probes was done in the 1960's and 70's, as they were used on rocket-borne missions to investigate the ionosphere. Because of the high velocities involved, measurements had to be taken rapidly. It was hoped that resonance probes could quickly and easily measure the plasma density and electron temperature, without using the traditional Langmuir trace method.

Applying an oscillating voltage of variable frequency to a probe produces a subsequent increase in dc current. This increase in dc current was known as rectification current, which is effectively $\Delta$I in this thesis. Generally, the resonance was observed by plotting $(I_{ave}(x)/I_{DC}(x))$ versus $\omega/\omega_{p_e}$, where $x$ is one particular value of dc bias voltage (always $< \Phi_p$), $\omega$ is the probe driving

frequency and $\omega_{p_e}$ is the plasma electron resonance frequency.

An anomalous increase in $\Delta$I with frequency is observed as $\omega$ approaches $\omega_{p_e}$[41-43]. This electron resonance condition is found to be dependant on the tip size and dc bias voltage. Essentially, there is a series resonance between the sheath impedance, $Z_{sh}$, and plasma impedance, $Z_p$ The oscillating voltage across the sheath increases at resonance, thus causing an increase in $\Delta$I[42].

The case of ion resonance, at $\omega \approx \omega_{p_{ion}}$, is perhaps more important for this thesis, as rf plasmas are operated below $\omega_{p_e}$. The sheath is modeled as an equivalent circuit of inductors (ion/electron inertia), capacitors(displacement current across the sheath) and resistors(convection, real current). Rosa [44] showed that ion transit times across the sheath are important, and derived an equation to calculate the components of the equivalent circuit as a function of frequency. Oliver and Clements [45] later showed good experimental agreement with Rosa's theory. However, there is still some debate as to the validity of these sheath models near ion resonance. Bhohk *et al* [46], showed how the previous inconsistencies can be resolved by using the 'dynamic Bohm criteria' (DBC), which takes account of the movement of the sheath edge and also the plasma inhomogeneities near the plasma-sheath boundary. This provides a condition for the appearance of ion resonance which can essentially be controlled by the applied dc voltage to the probe. This helps explain why ion resonance is observed in some experiments and not others ([47] for example)[48].

It should be noted here that in most of the above referenced literature, the experiments were usually conducted with the probe biased close to the floating potential or in ion saturation. For a review of early resonance probe theory, refer to [43].

The work on resonance probes is important here as it shows that there should be an anomalous increase in the measured $\Delta I(V)$ as either $\omega_{p_{ion}}$ or $\omega_{p_e}$ is approached. Comparing the actual distortion, $I_{ave}(V) - I_{dc}(V)$, with $\Delta I_{Harm}(V)$, will show if $\Delta I(V)$ can still be accurately determined by the sum of *even* harmonics, despite the voltage amplification at resonance.

## 4.7 Summary

The results from the simulation agree with the mathematical model. Ultimately, it has been shown that separating the ac and dc current components, using the circuit of figure (4.1), allows the time-averaged distortion component, $\Delta I(V)$, to be separated from the uncompensated dc current. Not only does this allow the undistorted effective dc I-V characteristic to be obtained without compensation, but also, for the first time, a reconstruction of the phase-dependant characteristics is possible.

The magnitude of the oscillation is unimportant provided the probe current does not perturb the plasma, and, the technique can be used in situations where adequate compensation is a practical impossibility.

It has also been shown that it is possible to accurately measure the time-dependant plasma potential (even if it is non-sinusoidal in nature) and also allows the phase-dependant nature of the plasma parameters to be explored, such as, $T_e(\phi)$, $n_e(\phi)$, $f(E, \phi)$ and as well as local measurement of ac electric fields Other phase-dependant measurements also become possible, such as, separating the real and imaginary components of the sheath impedance.

The effect of phase shifts were shown to be important, but can be removed during data analysis.

The loading effect of the measurement circuit also needs to be taken into

account. At low density and with a better circuit design, the loading effect should be negligible

Frequency effects and how these can potentially change the non-linear behaviour of the sheath has also been mentioned. However, this area is still relatively unexplored in detail, for the case of a small un-driven probe sheath. Because of this, is it not easy to predict the nature of the sheath impedance as frequency is increased. However, it should be possible to explore the phase-dependant characteristics as a function of frequency, thus potentially validating or extending present theories on non-linear sheath behaviour.

The anomalous increase in $\Delta I$ due to resonance may also demonstrate if it is possible for the harmonic amplitudes to increase without a corresponding increase in $\Delta I$. If this 'de-coupling' can be observed, then it would imply that the dc component is not always linked to the harmonics in the apparently fundamental way described above. The experimental investigation should shed more light on this issue.

# CHAPTER 5

---

# Experimental setup

---

The experimental set-up and difficulties involved in measuring the harmonics and resultant phase-dependant I-V characteristics are explained in this chapter, but first, the experimental chamber is described.

## 5.1 The Experimental Chamber

The experimental reactor used in this thesis (Applied Radio-frequency Ion Source or ARIS) was originally designed for the study of low temperature plasma chemistry [40] and has also been used in other studies, such as investigation of collisionless heating[49]. It is an inductively coupled rf discharge ignited in a small source region. The source is open at one end to a much larger chamber, into which the plasma diffuses. Most of the experimental results in this thesis were performed in the diffusion region of this cham-

ber. The large grounded area ensures that the plasma oscillation amplitude is fairly low, generally less than $T_e$. This allows the probes to be driven at various frequencies and amplitudes without much interference or 'contamination' of results by the plasma driving oscillation. The fact that the chamber grounded area is large also means that the plasma-ground sheath can essentially be ignored in calculations of sheath impedance.

### 5.1.1 Reactor geometry

The reactor consists of two distinct regions as shown in figure 5.1[49]. The source region is made from a dielectric tube with an external diameter of 100 mm, wall thickness 10 mm and length 150 mm. The rf power is coupled to this region with a two turn antenna which encompasses the source tube. The whole region is also surrounded with an aluminium electrostatic shield to prevent rf radiation escaping. The aluminium shield still permits the application of the dc magnetic field if desired. Probe access to the source region is also possible but the high density and temperature limits the life-time of probes in this area.

One end of the source tube is open to the expansion region which is made from stainless steel and has numerous vacuum feed-through ports which allow diagnostic access to different regions of the plasma. It has an internal diameter of 410 mm and is 290 mm long. It is closed at both ends with either stainless steel or aluminium end plates depending on the application. The source tube attaches to one end through an aperture with a diameter equal to the outer diameter of the source tube. The electrostatic shield mounts directly to this plate to hold the source in place.
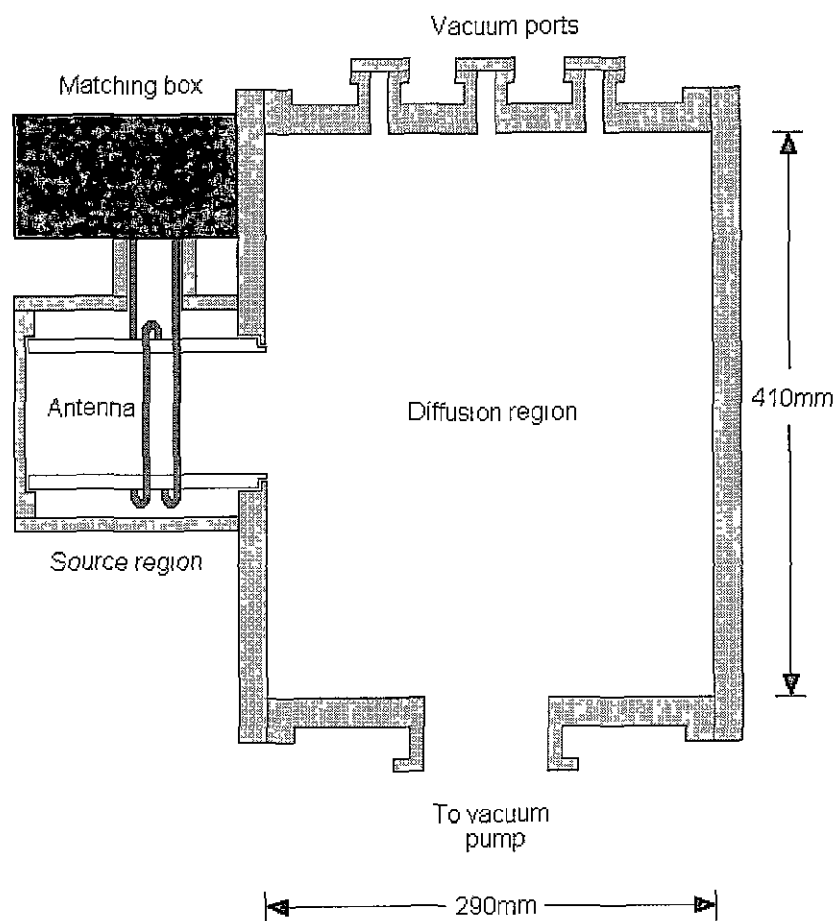
**Figure 5.1:** *Schematic of the ARIS device showing source and diffusion regions.*

## 5.1.2 RF power coupling

Radio frequency current at 13.56 MHz is driven through the antenna with an RFPP (Radio-Frequency Power Products) 3 kW generator. The antenna impedance is matched to the generator output impedance (50 $\Omega$), using a matching network, to achieve maximum power transfer.

The matching box is situated to allow direct connection of the antenna to the output capacitor of the match network. This minimizes ohmic power loss at the antenna side of the matching network. The match box is used

in automatic matching mode so that the power delivered to the discharge is held constant.

The source needs to be air cooled as some of the rf power is dissipated in the antenna itself. At high frequencies the resistance of the antenna increases due to the skin effect and is accompanied with power dissipation. Ion bombardment of the source walls also leads to heating of the source region.

The discharge is ignited initially in capacitive mode by the large rf voltage on the antenna. When the plasma density increases sufficiently the discharge moves to an inductive mode and is sustained by the time varying magnetic field associated with the rf currents through the antenna.

Most experiments were performed at 300W RF, as this was a stable operating point with mostly zero reflected power for extended periods of operation.

### 5.1.3 Vacuum system

The gas used in all experiments is Argon. Gas is fed to the large chamber using a mass flow controller rated at 100 SCCM and pumped with a turbo-molecular pump backed with a rotary pump. The base pressure of the system is $\approx 1 \times 10^{-6}$ mbar, while for most experiments, the operating pressure was in the mid-range of $1 \times 10^{-3}$ and $1 \times 10^{-2}$ mbar $\approx 1 - 10$ mTorr. This was the pressure range for which the plasma and matching unit was most stable, thus allowing repeatability. Under these conditions, the plasma density and electron temperature in this chamber are know to be about $4 \times 10^{15} m^{-3}$ and $\sim 4$ eV, respectively. Thus, the mean free path ($\lambda$) for electron-neutral momentum transfer is about 20 cm. This is clearly much larger than the sheath width or probe radius, so the probe is essentially operating in the collisionless regime.

Generally, the gas flow is held constant and the pressure is adjusted using a large gate valve mounted between the turbo pump and the chamber.

## 5.2 Diagnostic Set-up

### 5.2.1 Probe Design

Due to the nature of the required measurements, shielding from rf noise is very important. Electrically, the dc biased probe is only in contact with the plasma at the tip and we do not want stray pick-up along the length of the probe body, due to capacitive coupling. To avoid this, the probe is constructed from 50$\Omega$ semi-rigid coax cable. The outer shield is grounded while the inner core acts as the dc biasing and rf measurement line. The coax is protected from the plasma by placing it in a ceramic tube. Castable ceramic is used to prevent contact between the plasma and grounded coax shield of the probe. The tungsten tip is held in physical contact with the core of the semi-rigid coax, thus providing electrical connection between tip and biasing supply. The tip is also fully removable so that it can be replaced easily, without need for probe reconstruction. The vacuum seal is made on the outside of the chamber with epoxy. A diagram of the probe is shown in figure(5.2).

As can be seen from figure(5.2), the shielding extends right to the very base of the exposed tip. This provides complete shielding along the entire length of the probe. Testing the probe in an rf plasma, with and without a tip, shows that the amount of rf pick-up through the shielding is negligible.
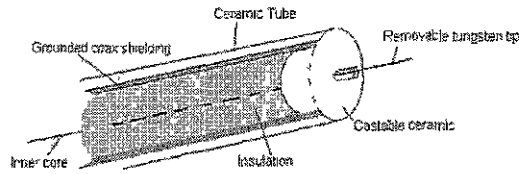
**Figure 5.2:** *Schematic of the rf shielded Langmuir probe.*
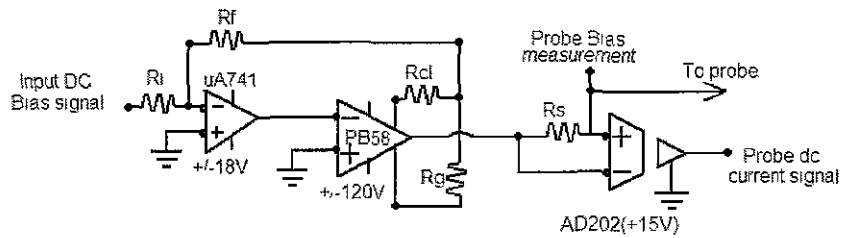


**Figure 5.3:** *Schematic of the Langmuir probe measurement circuit.*

## 5.2.2 Langmuir probe circuit

The standard Langmuir probe circuit for measuring the dc I-V characteristics is shown in figure 5.3. The isolation amplifier is used to avoid grounding the probe biasing supply.

## 5.2.3 Modified circuit

The simulation of the originally proposed circuit (**Section 4.4**) showed that a 'loading' effect may be observed due to the measurement resistor. To avoid this situation, the circuit was modified slightly to that of figure (5.4).

The sense resistor has been replaced by a 'pick-up' current sensor, allowing the same rf current measurements to be made without a loading resistance. Because the sensor interacts with the rf current-induced magnetic
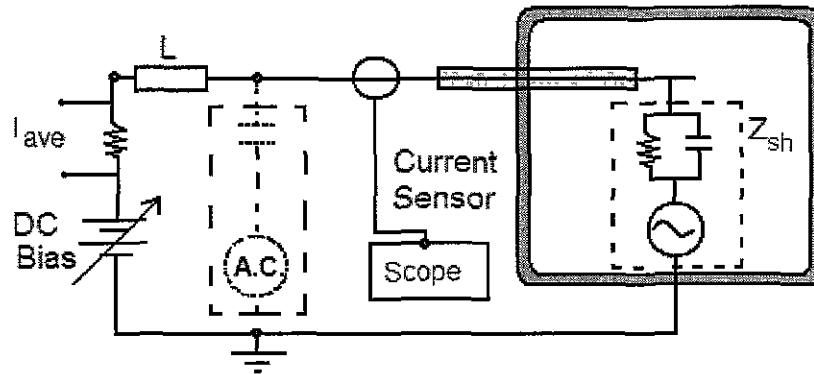
Figure 5.4: *Schematic of modified circuit for reduced 'loading'. The a.c. generator and capacitor are necessary only if the probe is driven to replicate plasma potential oscillations.*

field, there will always be some degree of loading, however, according to the manufacturer (Tektronics, CT1 current sensor) the insertion impedance is less than 1 $\Omega$, therefore loading effects should be negligible. The CT1 sensor has a bandwidth of 25 kHz to 1 GHz and a gain of 5mV per mA, with 3 % accuracy. The sensor is capacitive in nature, so no dc component of the rf oscillation is measured. The circuit inductor is necessary to prevent the time-varying current from effecting the d.c. supply.

In these experiments, the oscillation amplitude of the plasma was quite low, generally < 3 V, so the a.c. generator was used to drive the probe over a range of known frequencies and amplitudes The circuit capacitor stops the d.c. signal affecting the a.c. supply.

Finding suitable inductors with sufficient impedance at low frequency (< 200 kHz) was difficult, so shunting capacitors were used to further decrease the amplitude of a.c. signals reaching the d.c. supply. Although the current may be heavily shunted here, the current measured through the current

sensor is still accurate because of where it is positioned in the circuit. Effectively, the current from the a.c. generator takes two paths, one through the inductors (and then shunted to ground, not shown in diagram), the other flows to/from the probe tip. This is the current of interest and is measured by the sensor. However, because the probe is coaxial in nature, with the outer shield grounded, the a.c. current also finds a path to ground through the probe shield. This *stray* current can be measured directly by turning off the plasma while the a.c. potential drives the probe. This stray current is subtracted from the total *plasma on* current to reveal the desired current.

A *double-shielded* probe was also constructed to eliminate the stray current. Essentially, this consists of the same semi-rigid coax line, surrounded by insulator(ceramic), all encased in a grounded metal shield (tube). The coax shield is capacitively coupled to the core (signal carrying line) and is driven at the same potential as the tip, thus, no capacitive coupling between the measurement line and the coax shield can occur. The sensor only measures current through the core, thus, only current through the plasma-probe tip is measured. The outer shield is grounded and is needed to prevent the plasma from being distorted by the large-area driven shield.

The double-shielded probe is only required in this case because the probe is driven in order to increase the sheath oscillation. In plasmas with larger potential oscillations, the single-shielded probe would be sufficient.

In order to collect meaningful data, it is necessary to have a stable reference signal for triggering the measurement channel of the scope. This reference signal can be obtained by placing a *pick-up* probe inside the plasma. This can be a simple *floating probe* with no bias connection. The signal is taken directly from the probe to a high impedance scope. Alternatively, a signal from the rf source driving the plasma could be used.
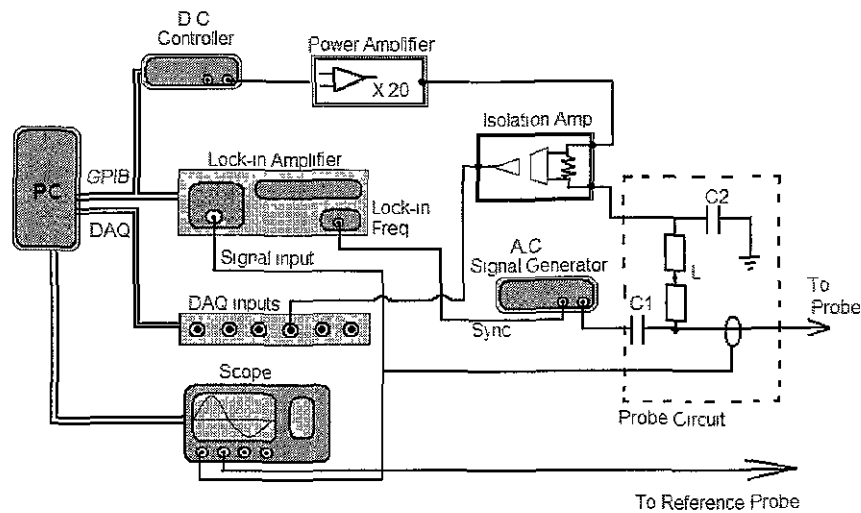
**Figure 5.5:** *Schematic of Lock-in amplifier circuit for second harmonic measurement and also the set-up required to measure and record the rf waveform signals.*

## 5.2.4 Harmonic Measurement circuit: Lock-in Amplifier

A lock-in amplifier was used to measure the second harmonic amplitude. The complete circuit is shown in figure (5.5).

The signal generator drives the probe with an a.c. potential. The lock-in amplifier takes the signal from the current sensor and a reference input frequency signal from the sync output of the probe driving generator. The lock-in amp(Stanford Research Systems, SR844) had a minimum operating frequency of 26kHz, resulting in a minimum second harmonic frequency of 52kHz. Synchronizing another signal generator can be used to measure higher harmonics such as $f_4$, $f_6$ etc. One is used to drive the probe, while the other acts as the reference signal for the lock-in amplifier (this is not shown in figure(5.5)).

For nearly all measurements, only the second harmonic was used as it

was found that the higher *even* terms were very small in amplitude and had little effect on $\Delta I(V)$. The maximum amplitude of the second harmonic is obtained at each bias voltage. This information can be plotted directly, using the data analysis software written in LabView. Using this set-up is very simple as issues with phase are eliminated when only the $f_2$ amplitude is used

As figure(5.5) shows, the second harmonic from the current sensor signal is measured on the lock-in amplifier, while simultaneously the waveforms are measured on the scope and recorded by the computer. The effective dc and time-averaged I-V characteristics are measured through the Langmuir probe circuit. This set-up allows measurement of $\Delta I(V)$ and $I_{ave}$ as a function of frequency and amplitude.

The effective dc characteristic, $I_{DC_{eff}}(V)$, is obtained by dc sweeping the probe only, i.e. *no superimposed ac probe-driving signal*. In this case however, there may still be a small oscillation due to the plasma driving oscillation. To reduce its impact, and thus obtain greater dc accuracy, tuned inductors at 13.56MHz were placed near the tip (for dc measurements only). These inductors were removable, without having to break the vacuum seal or turn off the plasma, which allowed measurements to be quickly taken for compensated (undriven) and uncompensated (driven) probes. Removable inductors are only necessary here to provide a dc reference characteristic to prove this ac technique. Thus, the actual experimental $\Delta I(V)$ is given by $I_{ave}(V) - I_{DC_{eff}}(V)$. This is compared with $\Delta I_{f2}(V)$. Any error in $I_{DC_{eff}}(V)$ could be mistakenly interpreted as an error in the analysis, so d.c. accuracy is important here.

Further inductors were also necessary, as shown in figure(5.5), to prevent the driven oscillation signal from entering the dc bias line. This was crucial,

as without them, not only was the dc supply voltage affected, but it also caused major distortion to the measured I-V characteristics.

## 5.2.5 Probe Calibration

Cable lengths between the probe and measurement devices can cause both amplitude and phase distortion of the measured signals. In this system, there are two main causes of phase distortion, one is caused by line length, the other, by changes in sheath impedance with bias voltage.

Although different frequencies in a measured signal all travel at the same speed through the cable, differences in wavelength result in an overall phase shift of the total signal. This phase-shift is a function of cable length, frequency and velocity of the signals through the cable. The velocity factor, $v_f$, is the ratio of the signal velocity in the cable to that in vacuum. It is therefore always less than one. For the semi-rigid coax used to build the probes(RG402), $v_f$ is 0.68.

$$\Delta\phi = (L/(v_f * c)) * \omega \tag{5.1}$$

where; L = coax line length; $v_f$ = velocity factor; c = speed of light in vacuum; $\omega = 2\pi f$,

From equation (5.1), it is clear that phase-shift increases with frequency and line length. Thus, the measured signal cannot be an exact replica of the signal at the tip. Calibration will remove the phase-shift due to line length, but not the phase shift due to changes in the sheath capacitance, as this is unknown before the measurements are recorded.

### 5.2.6 Probe Calibration for Line Length

The probe is calibrated on the bench for amplitude and phase by applying a variable frequency signal at the tip of the probe while monitoring both input and output signals. This is similar to the technique used by Sobolewski and is described in detail elsewhere[50].

The signal generator outputs a sine wave (starting at the fundamental), while both input and output waveforms are collected. The amplitude scaling factor is found from the ratio of input to output voltage. The phase difference between the signals is measured directly, either by the scope or through the data collection software. The frequency is then incremented to the next harmonic and the procedure is repeated, thus mapping the phase and amplitude calibration factors of the probe system over the frequencies of interest.

Calibration of this probe presents some difficulties however, as due to its construction, the shield near the tip cannot be grounded directly at that point because it is housed inside the ceramic. Thus, during calibration, the probe may be poorly grounded along its length. To overcome this, the probe was housed inside a metal tube of slightly larger diameter, which could then be grounded at both ends.

Using the grounded metal 'shield' effectively provides a better ground connection over the entire length of the probe, thus eliminating any stray capacitance effects which distort the calibration signals. Phase shifts for the probe were recorded and compared with measurements for an equal length of ordinary coax cable. Both measurements were in approximate agreement, indicating that the probe calibration method is correct, and also showing that the probe essentially acts like a transmission line.

### 5.2.7 Sheath Impedance Phase Correction and FFT's

The measured a.c. signals, now corrected for line length distortions, should be identical to the signals found at the tip, however, the phase change due to the sheath still has to be accounted for. To correct for the sheath-induced phase-shifts, the following procedure is used:

The complex FFT for each waveform is used to calculate the absolute value of amplitude for each relevant harmonic. The phase relative to zero for each harmonic frequency is calculated from equation(4.1). Sine waves of the appropriate amplitudes and phase for each harmonic are thus constructed for each point in bias. The phase of the fundamental is set to zero, so the appropriate phase for each harmonic is then determined by $\phi_{f1} \times f_n$, where $\phi_{f1}$ is the original fundamental phase and $f_n$ is the harmonic number. For example, if $\phi_{f1} = \pi/4$ (at a particular bias), then $\phi_{f2}$ and $\phi_{f3}$ would be $\pi/2$ and $3\pi/4$, respectively. The resultant waveform is the sum of these replicated sine-waves and has an identical shape to the original waveform, but simply shifted so that its fundamental starts at zero phase. This is repeated for each bias and thus eliminates any phase-shifts between waveforms measured at different bias voltages.

The effect of energy spreading in the Fourier analysis was greatly reduced by choosing an appropriate number of samples, N, such that, $\Delta f/f$ is as close to an integer as possible, where f is the fundamental frequency of the measured signal and $\Delta f$ is the frequency resolution of the system, given by

$$\Delta f = (\Delta t/N) \tag{5.2}$$

where $\Delta t$ is the sample rate.

Another important point about manipulating the FFT data is that the calibration factors for amplitude and phase must be applied to the full com-

plex FFT array. The amplitude values must be scaled at both ends of the array, while the phase-shifts must be applied with the same magnitude but of opposite sign to the first and second halves of the array. The correct waveforms are then found from the inverse FFT of the corrected array.

## 5.2.8 Data Collection

LabView programs were written for automated control of the probe and to collect all the generated data. The main programs used were for rf waveform measurements, collecting harmonic data from the lock-in amplifier and collecting DC and time-averaged I-V characteristics from the Langmuir probe. Both ac and dc sources were controlled by the program, while the measurements were recorded from an oscilloscope connected to the computer through a GPIB connection. For the Langmuir trace measurements, a DAQ card was used to collect the data, again controlled through LabView.

For the rf waveform measurements, the dc voltage sweep and scope settings were all controlled by the program. For more accurate readings, the scope was autoset after each voltage increment and the scaling measured and adjusted accordingly by the program to provide maximum sensitivity for weak signals. The measured rf waveforms were averaged up to a maximum of 512 times, but in order for this to be effective, a sufficient time delay between voltage increments was included. Results from the calibration are read in from a file and used to manipulate the incoming waveforms, thereby removing the distortion effects of the probe system. The fundamental phase of these signals is measured, and compared with the phase of the reference signal, for later manipulation.

There are various methods of sweeping the voltage signal, however, the easiest and most effective in this case is to simply increment the voltage,

average the waveforms sufficiently, capture the waveform data and then continue incrementing the d.c. bias voltage. This approach is slow. A faster and more accurate data acquisition was not available at the time.

The rf measurement program also calculates the FFT's and plots rf waveforms against time and bias voltage. RF I-V traces are generated on-screen for quick comparison. All data collected is written to a file accessible by Matlab for further in-depth analysis.

## 5.3  Summary

The experimental chamber and plasma have been described. Many of the experimental difficulties, such as calibration and FFT issues have also been pointed out. The design of the probe is also very important, as capacitive coupling must be prevented between the plasma and probe body, as the only signal that should be measured is the one at the tip. The shielding is sufficient to achieve this.

The fact that the probe no longer acts like a correctly terminated transmission line when the $50\Omega$ resistor is replaced by the current sensor will change the amplitude and phase of the signals measured. The amplitude attenuation and phase distortion caused by line length must be calibrated out so that the measured signals are not distorted by the measurement system.

The main circuit for data collection uses the lock-in amplifier, dc and rf I-V measuring circuits to obtain the rf I-V characteristics, dc and time averaged traces. $f_2$ is measured directly, while capturing the full rf waveforms as a function of bias voltage also allows all significant harmonics to be measured via FFT.

The phase shifts are problematic for reconstructing correct rf I-V charac-

teristics but the methods discussed can be used to overcome this.

The data collection system is comparatively slow, but works well enough to obtain experimental results largely in agreement with the simulated data. The experimental results are explored in the next chapter.

# CHAPTER 6

## Results

In this chapter, the experimental results are presented and compared against the simulated data of **Chapter 4**. The experimental set-ups used to obtain these results have already been described in the previous chapter.

## 6.1 Measuring $\Delta I$

Figure(6.1) shows the second harmonic amplitude as a function of bias voltage for a 26kHz, 10V amplitude oscillation driven on the probe tip through that of circuit (5.5).

Comparing figure (6.1) to the simulated data, the trends are clearly very similar. The absolute value of the $f_2$ amplitude is the actual measured quantity. The values shown as dots were obtained by taking account of the appropriate polarity at the inflection point, as described previously.
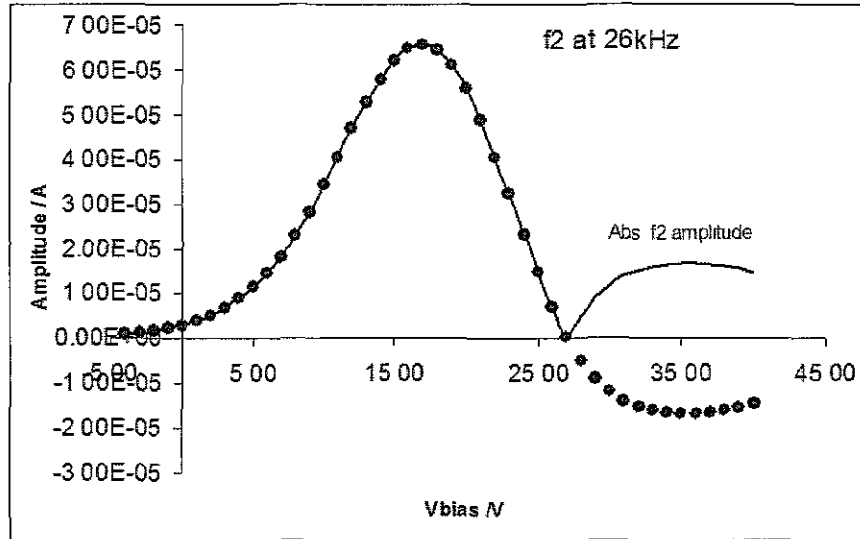
**Figure 6.1:** *Experimental second harmonic amplitude versus bias, measured on lock-in amplifier. The probe was driven with a 10V 26kHz signal. The absolute value is shown also as this is the actual measured signal.*

It was also found that there is a strong discontinuity in the measured harmonic phase at the inflection point. This is shown in figure (6.2) for various frequencies. This phase change can also be used to clearly determine the point at which the harmonic amplitude changes polarity. Near ion resonance however, the phase response becomes more complicated, as shown at 1.5 MHz.

Figure (6.3), shows the I-V characteristics obtained via the I-V recording circuit/system. The dc characteristic is obtained using a compensated probe with no applied ac probe signal. Technically, because the oscillation amplitude of the plasma potential is known to be small in this chamber(~ 3 V), the use of compensation inductors is not totally necessary. However, a slight difference between compensated and uncompensated dc traces was observed under certain conditions, so for accuracy and repeatability, the compensated
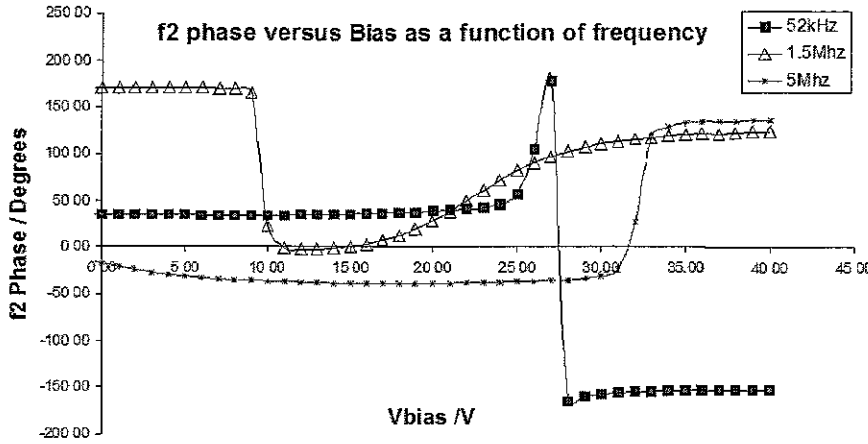
**Figure 6.2:** *Experimental second harmonic phase as a function of bias, at various frequencies. The discontinuity marks the change in polarity of the $f_2$ signal.*

probe was used for all dc traces.

The time averaged trace was recorded without any compensation. Swapping between compensated and uncompensated probes was very quick and easy, thus the plasma did not change appreciably during the interval. Also, because the same probe tip was used, the two resulting traces could be directly compared.

It is clear from figure(6.3) that the dc trace is distorted by the presence of the oscillation applied to the probe (11 MHz in this case). Although, the oscillation amplitude is not excessively large relative to the approximate electron temperature value of 4.5eV, the time-averaged effect is still significantly pronounced.

As explained in previous chapters, the theory suggests that subtracting $f_2(V)$ from $I_{ave}(V)$, should correct for the time-averaged distortion and reveal the undistorted effective dc trace. This is clearly proven in figure(6.3). The agreement is excellent. The electron temperatures calculated from the effective dc trace and the corrected trace were measured and compared. The
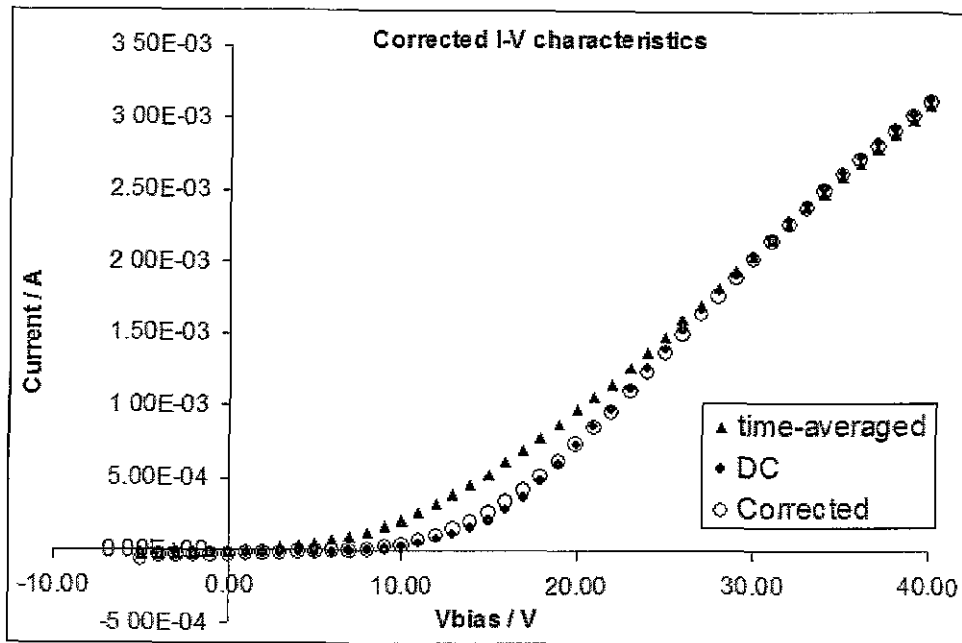
**Figure 6.3:** *Experimentally measured dc and time-averaged characteristics. The corrected trace, $I_{ave} - f_{2amp}$ is shown to replicate the dc trace very accurately. The amplitude and frequency of the applied oscillation are $10V$ and $11MHz$, respectively.*

difference was less than 0.4 eV approximately. However, due to the inaccuracy of the current measurements in both dc and corrected traces it was difficult to determine accurate $T_e$ measurements.

### 6.1.1 Frequency Effect on experimental ΔI

Figure (6.4) shows the effect of frequency on the measured $f_2(V)$ signals. The result at 1.5MHz is extremely distorted and is not shown to maintain clarity of the figure. $\omega_{p_{ion}}$ was calculated to be approximately 1.5MHz for these plasma conditions, so the distortion must be due to ion resonance. Ion resonance is known to be quite broad, so the results between 400kHz and 2MHz are in agreement with this as they do not have the predicted shape of ΔI(V). The results outside of resonance, at 26 kHz and 4.5 MHz are in good qualitative agreement with the simulation and show clear inflection points.

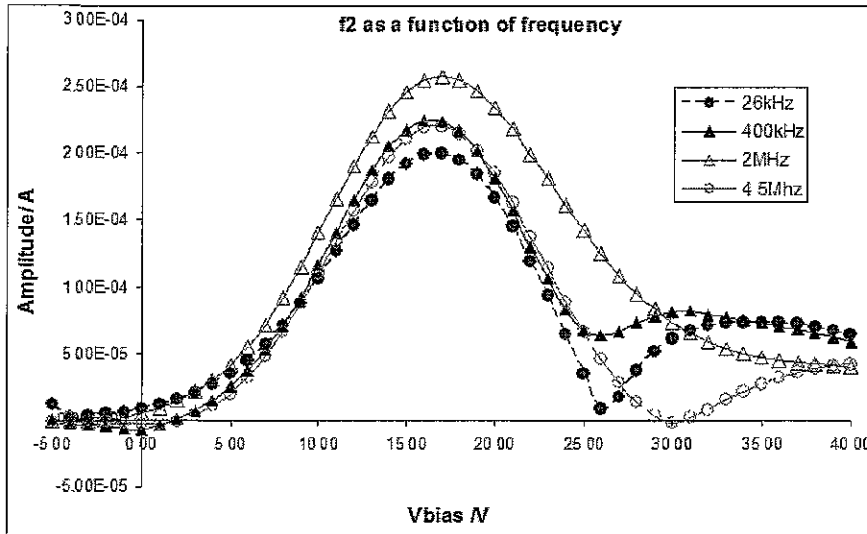

**Figure 6.4:** *Abs(f₂) versus bias, as a function of probe oscillation frequency*

Aside from illustrating the resonance condition, figure (6.4) also shows that the behaviour of ΔI(V) does not change significantly at high frequencies.

The only obvious difference is that the inflection points are shifted to higher bias voltages at higher frequencies(outside of resonance).

It should be noted here that some points on figure (6.4) appear negative at low voltage, eventhough the absolute values are used, this is due to an offset error on the lock-in amplifier, caused by stray current coupling through the grounded shield. Generally, this error was relatively small and did not represent a major problem.

The approximate value of the oscillation potential is given by the bias separation between the ΔI(V) peak-to-inflection points. This can be clearly seen in figure(6.4) 26 kHz results, where the oscillation was 10 V. For low frequencies, the oscillation amplitude is approximately predicted, but at higher frequencies the results indicate that the oscillation amplitude has increased. This may be due to errors in calibration.
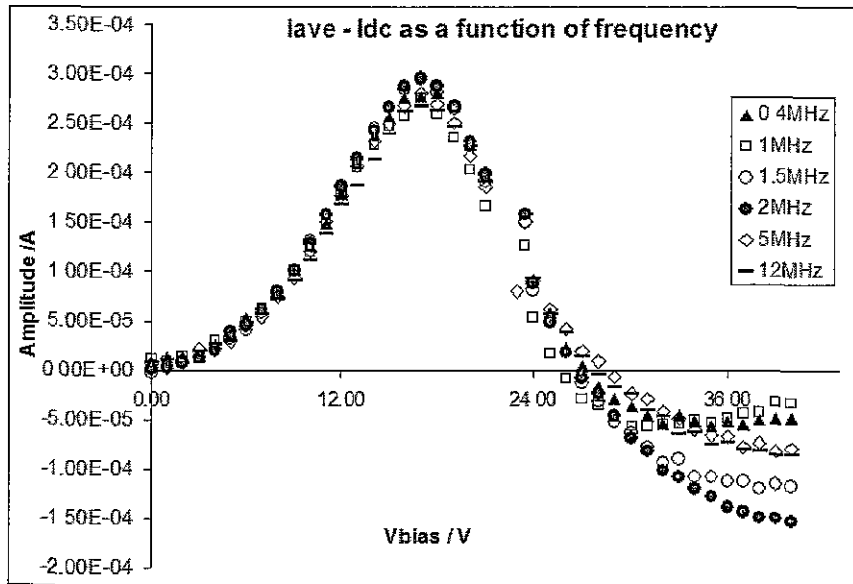


**Figure 6.5:** *Change in ΔI(V) ($I_{ave}(V) - I_{DC_{eff}}(V)$) as a function of frequency. $I_{DC}$ is unchanging, so the time-averaged characteristic is clearly a function of frequency, as expected.*

Assuming $f_2(V)$ replicates $\Delta I(V)$ reasonably accurately, then any changes in $f_2(V)$ as a function of frequency (figure 6.4) must also be apparent in the resultant time-averaged traces. To put these changes in context, the time-averaged and dc traces were recorded under the same conditions, as a function of frequency. The actual $\Delta I(V)$ curve is given by $I_{ave}(V) - I_{DC_{eff}}(V)$, these are shown in figure(6.5).

The most important point to note from figure (6.5) is that the low and high frequency cases are again in approximate agreement with each other but near ion resonance (2 MHz data), there is a clear deviation away from the low and high frequency $\Delta I(V)$ results, particularly in the electron saturation region.

This implies that resonance affects both the $f_2(V)$ amplitude and the time-averaged I-V characteristic. However, $f_2(V) \neq \Delta I(V)$ near resonance, so this suggests that the sheath-generated time-averaged components are no longer directly coupled to the harmonic amplitudes.

A direct comparison of $\Delta I(V)$ and $f_2(V)$ at high frequency is shown in figure(6.6).

The greatest error between $\Delta I(V)$ and $f_2(V)$ occurs at the peak amplitudes. The simulation shows that including the amplitude of the $4^{th}$ harmonic should reduce this error, but experimentally the $4^{th}$ harmonic was found to be negligibly small. Therefore, the reason for this discrepancy between $\Delta I(V)$ and $f_2(V)$ is unclear.

The simulation was also used to demonstrate the effect of removing the phase-dependant ion current, which experimentally, occurs at high frequency. Because the current is mainly dominated by electrons, removing the ion current has little effect on the overall nature of the $\Delta I(V)$ curve. This is effectively demonstrated in figures (6.4) and (6.5) by the fact that both low
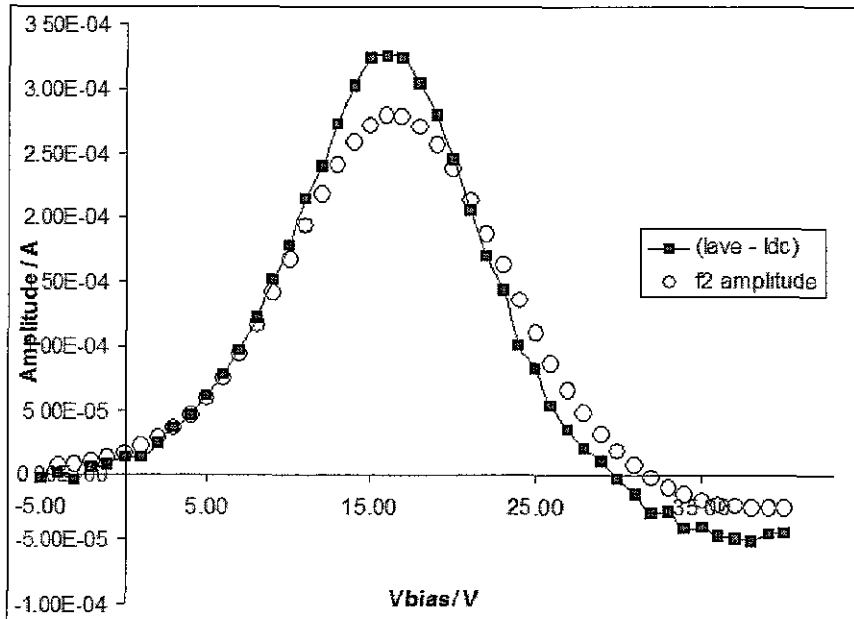
**Figure 6.6:** $\Delta I_{actual}(V)$ compared with $f_2(V)$, at high frequency (11 MHz). This is the $f_2(V)$ curve used to compensate the traces shown in figure(6.3)

and high frequency results are very similar at low bias voltages.

## 6.1.2 Amplitude effects on ΔI

The amplitude of applied oscillation was incremented at the end of each complete dc bias scan, while frequency was held constant. The results are plotted in figure(6.7) for a frequency of 5 MHz.

The peak values of $f_2(V)$ current scales linearly with oscillation amplitude. When the results are normalized for amplitude differences, it can be shown that the 'structure' of each curve is very similar. Only slight differences occur due to the fact that at the higher oscillation amplitudes, more regions of the I-V curve are explored. This is exactly as expected and shows that fundamentally the amplitude of oscillation has no detrimental effect on this analysis (as it does in the case of the a.c. technique for EEDF measure-
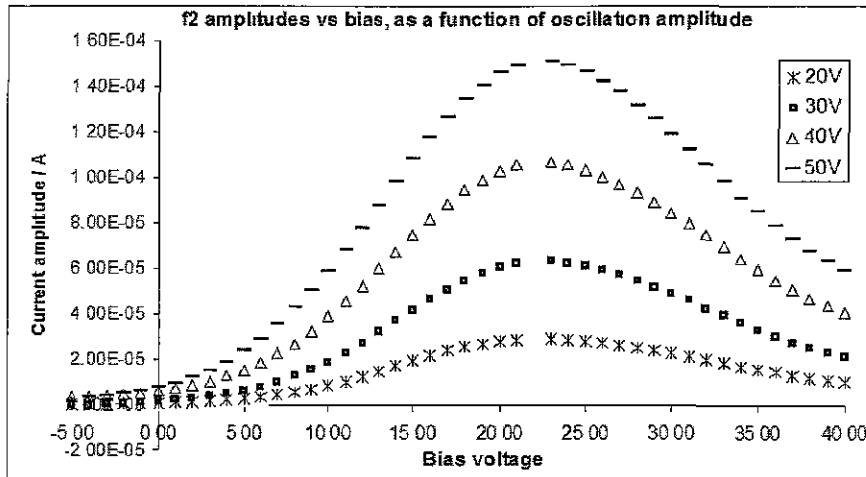
**Figure 6.7:** *Effect of increased amplitude of oscillation on the $\Delta I$ curve.*

ments).

It should be pointed out that the amplitudes shown on figure(6.7) are only the input oscillation values. The bandwidth of the amplifier effectively reduced the actual oscillation at the probe tip but the precise values are not important here.

## 6.1.3 Effect of collection area on $\Delta I$

By changing the tip size, it is possible to change the total sheath impedance and also the ratio of capacitive to real current The effect of this is demonstrated in figure 6.8.

The tip lengths used were 8mm, 4mm and 2mm approximately. The 2mm results are not shown as the high frequency measurements for small collection areas were unreliable. This is because the higher frequency results are much more susceptible to errors due to the *offset current* effect mentioned above. This problem is enhanced for smaller tip sizes and higher frequencies, as the signal to noise ratio decreases. Again, the apparent deviation into negative
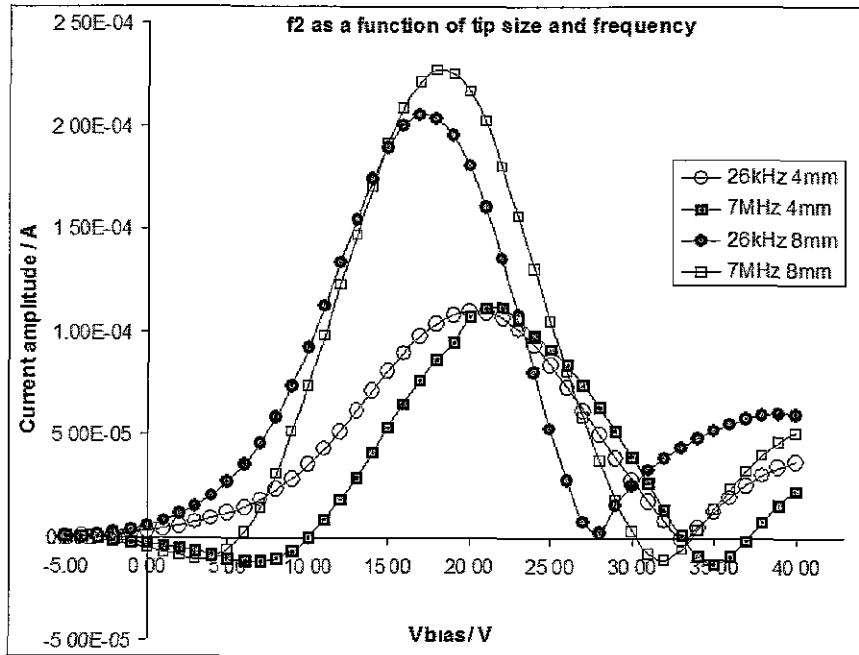
**Figure 6.8:** *Effect of changing tip size on ΔI. Shown at low and high frequency.*

values in figure (6.8) is only an experimental error due to this "offset current" problem.

At 8mm the results show that for the higher frequency of 7MHz, the $f_2(V)$ curve is wider than at 26kHz. This trend is repeated as tip length is halved. Thus illustrating again the slight change in behaviour of the $f_2(V)$ response at higher frequencies. The shape of $f_2(V)$ also clearly changes as a function of tip size for each frequency, thus indicating that the signal is not simply halved because the collection area is halved, but that the nature of the impedance itself is actually changed. This demonstrates a change in the ratio of displacement to real current.

## 6.1.4 Effect of pressure changes on ΔI

The pressure was varied after each $f_2(V)$ curve was collected. Figure(6.9)
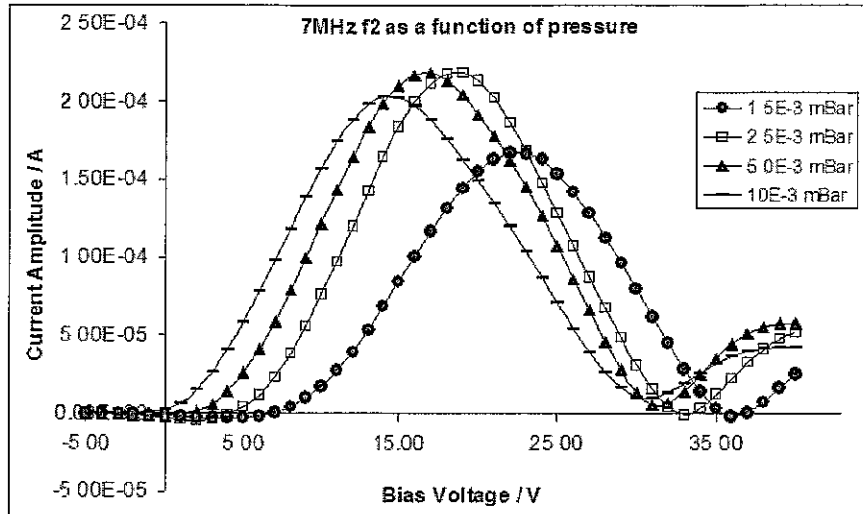
**Figure 6.9:** *Effect of changing the gas pressure on $\Delta I$. Shown at high frequency(7MHz).*

shows how both the peak and inflection points of the $f_2(V)$ curves appear at lower bias voltages as pressure increases. The actual shape of the curve does not change significantly over this pressure range. The pressure variation is quite small however, $1.5 \times 10^{-3}$ - $10 \times 10^{-3}$ mBar (1.125 - 7.5 mTorr) as the operating conditions were not very stable outside of this range. Nevertheless, a clear trend is observed. This also demonstrates how a small change in operating pressure during repeated measurements may cause a relatively significant change in the $\Delta$I(V) curve. This may help explain some experimental inaccuracies.

The simulation was used to better understand these results. A change in pressure causes a change in plasma density and electron temperature. If the electron temperature is increased, then the distortion effect of the same oscillation amplitude will be reduced (smaller $\Delta$I amplitude), while an increase in density causes a linear increase in total current (and $\Delta$I). Using the simulation it was found that the observed shift along the bias axis could

be replicated by a change in electron temperature, as shown by the simulated data of figure(6.10), where $T_e$ was varied for a fixed oscillation amplitude of 10 V and a constant density of $8 \times 10^{15} m^{-3}$.
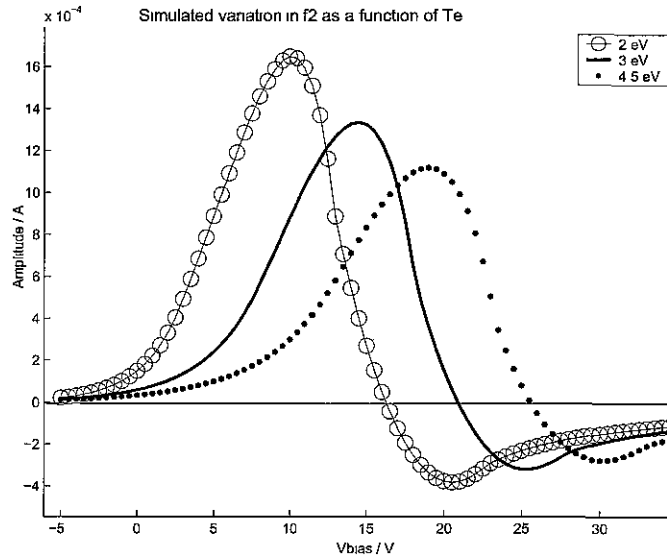


**Figure 6.10:** *Simulated effect of $\Delta I(V)$ as a function of Te.*

The exact ΔI(V) curve is thus particularly sensitive to electron temperature.

## 6.1.5 Experimental RF I-V and Phase-Dependant Characteristics

Figure(6.11) shows the experimentally obtained rf I-V characteristics at 0.2 MHz.

As figure (6.11(top)) shows, the t=0 trace yields ΔI(V) (highlighted by dots). This is inverted and expanded in figure (6.12). As can be seen, its shape is very similar to the expected ΔI(V) curve. This reconstructed ΔI(V) curve was added to the raw rf I-V characteristic to reveal the modified rf
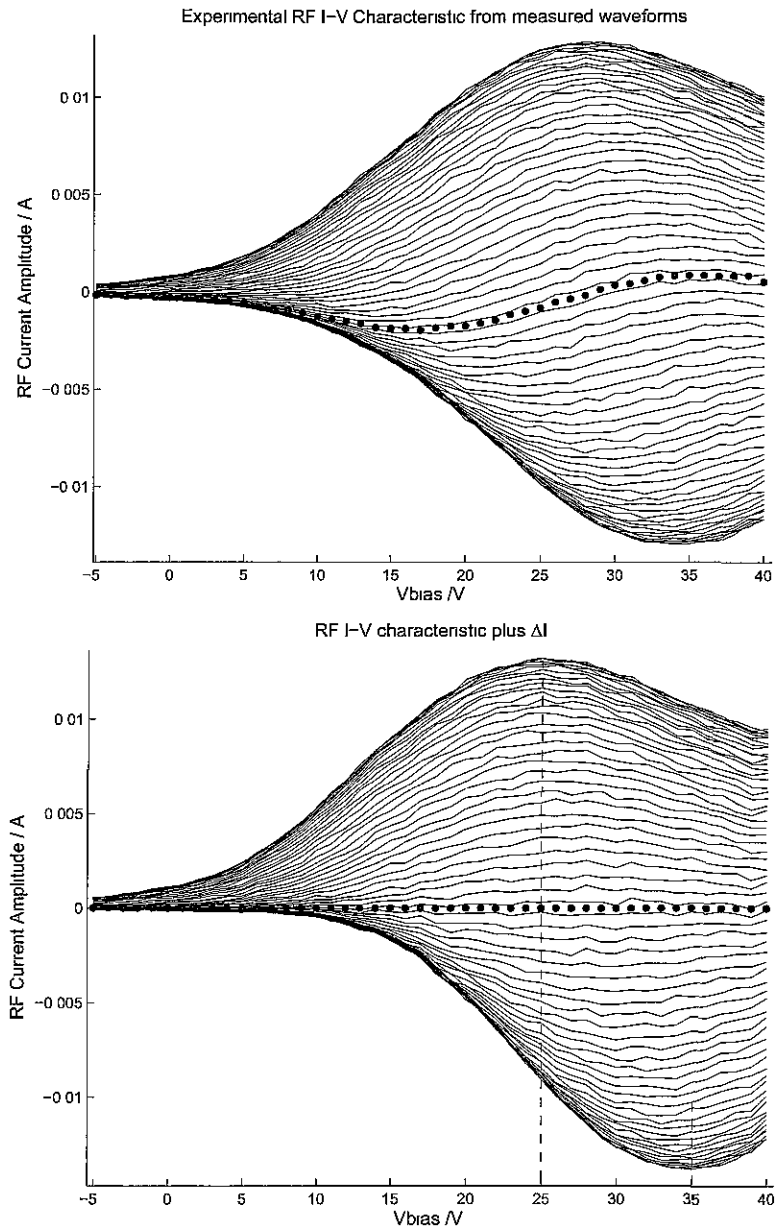
**Figure 6.11:** *Experimental RF I-V characteristics, 200kHz, 10V oscillation amplitude: (Top) Raw RF I-V characteristics from measured waveform data. (Bottom) Modified RF I-V characteristic with $\Delta I$ included. The $t = 0$ trace from the raw RF I-V characteristic (top) was used to obtain $\Delta I$.*
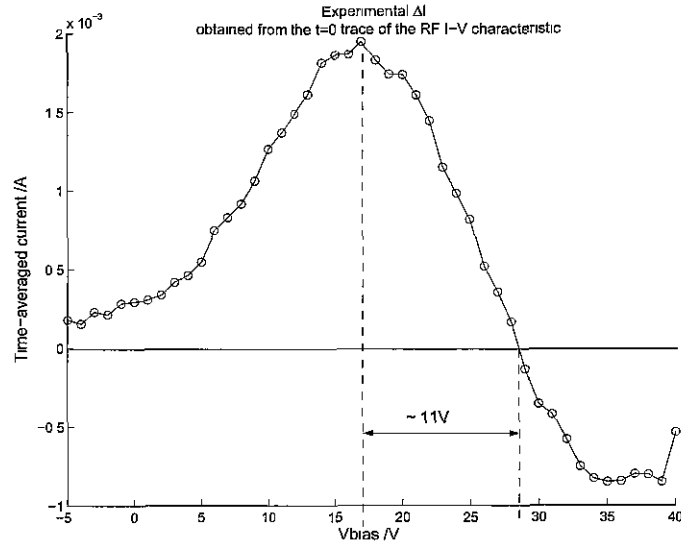
**Figure 6.12:** *Experimentally reconstructed $\Delta I$ from the t=0 trace of the raw RF I-V characteristics shown in figure(6.11(left)).*

characteristic of figure (6.11(bottom)). From this, the amplitude of oscillation is observed from the separation of the positive and negative peaks on the bias axis, exactly as predicted by the simulation. The correct amplitude of 10 V is clearly indicated.

Figure (6.12) also illustrates another prediction of the model - that the difference between the peak and inflection points on the $\Delta I(V)$ curve should also give the amplitude of oscillation. This is found to be approximately true, as a value of just over 11 V is found, instead of the correct value of 10 V. The data is noisy however, due to poor averaging and small signal amplitudes, but even so, the results are in excellent agreement with the simulated predictions for this technique.

The 200 kHz phase-dependant I-V characteristics of figure (6.13) are obtained by adding the data of figure (6.11(top)) to the time-averaged I-V characteristic shown as circles. Again this compares well with the simulated
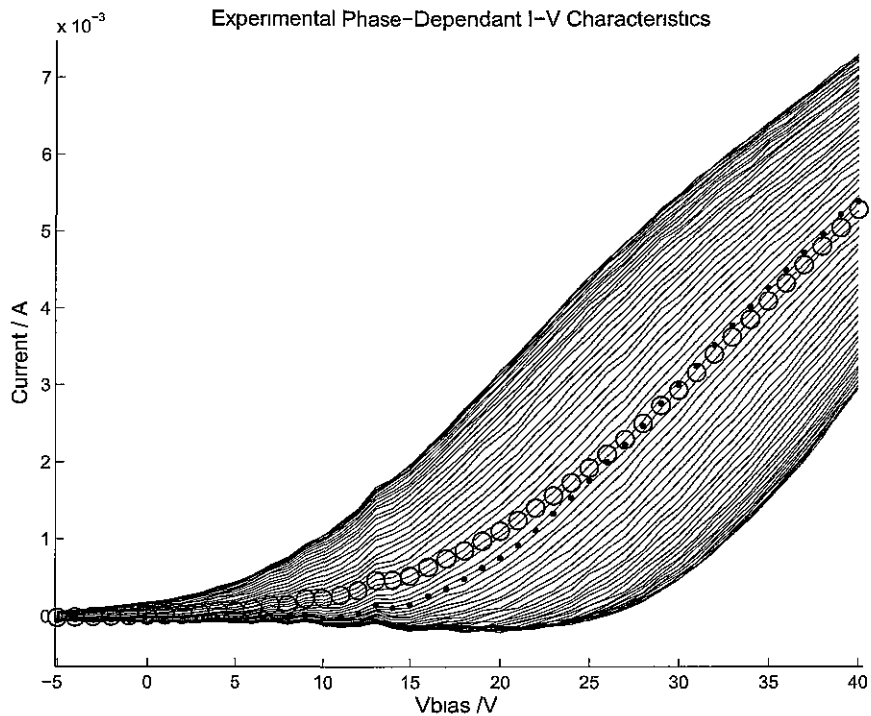
**Figure 6.13:** *Experimentally reconstructed phase-dependant characteristics at 200kHz. The solid lines represent the I-V characteristics at each point in phase of the oscillation. The circles mark the position of the time-averaged trace, while the dots are the dc (t=0) trace. The phase-dependency is created by the addition of $I_{ave}$ and the rf current of figure (6.11(top)).*
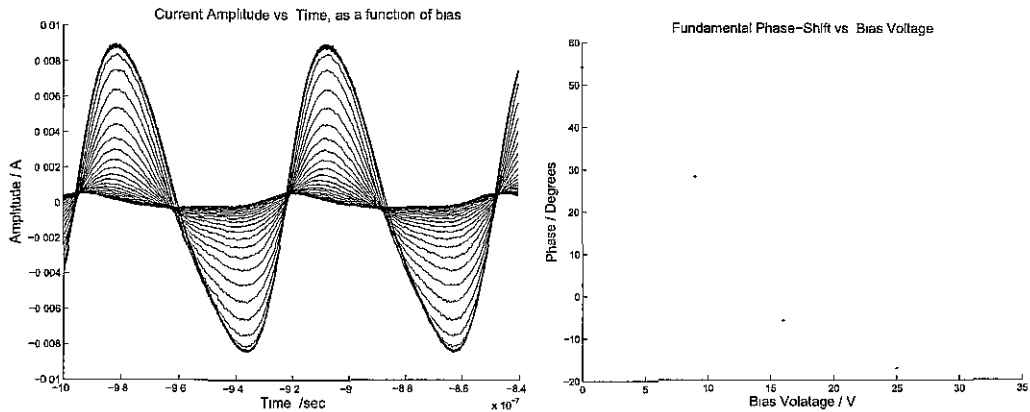
**Figure 6.14:** *Experimental RF data at 13.56 MHz with un-driven probe: (Left) Raw RF waveform data as a function of bias. (Right) Phase-shift in the measured fundamental waveform as a function of bias.*

predictions, demonstrating that this new technique can yield important data in a relatively simple way. Unfortunately, this data was too noisy to accurately obtain the phase-dependant plasma potential from the second derivatives, or indeed other phase-dependant parameters. A data collection system with better resolution and averaging would greatly improve the results.

Phase-dependant characteristics were also obtained at higher frequencies, up to 13.56 MHz, however, because the probe is driven, the stray current became excessive, making reliable measurements impossible. The double-shielded probe should overcome this effect but was found to produce spurious signals as the reflected power caused the output of the signal generator to vary. To demonstrate the feasibility of this technique at higher frequencies, an un-driven probe was used to measure the 13.56 MHz plasma current.

The raw rf waveforms at 13.56 MHz are shown in figure (6.14 (left)) as a function of bias voltage, while the associated phase-shift measured on the fundamental (13.56 MHz) as a function of bias voltage is shown in figure (6.14 (right)).

103
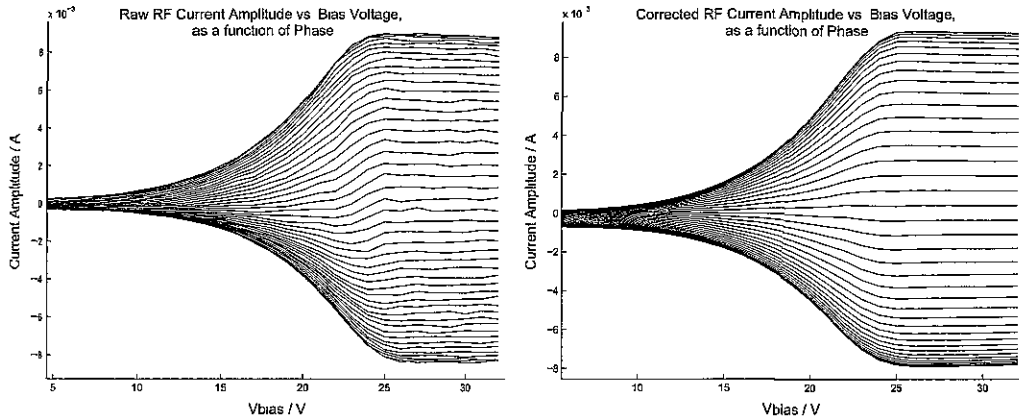
**Figure 6.15:** *Experimental RF I-V characteristics at 13.56 MHz with un-driven probe· (Left) Raw RF I-V characteristics from measured waveform data. (Right) Phase-corrected RF I-V characteristic.*

Figure (6.15) was constructed from the data of figure (6.14(left)) and shows the 13.56 MHz rf I-V characteristics before and after phase-shift correction. The corrected data appears to be less noisy because the correction procedure *re-builds* the waveforms with the appropriate amplitude and phase at each harmonic. This procedure was explained in 5.2.7.

Phase-dependant I-V characteristics at 13.56 MHz are shown in figure (6.16). The effective dc trace was measured with a compensated probe and is highlighted by dots.

The oscillation in the plasma potential was measured with a large-area floating probe and found to less than 5 V amplitude. The relatively small oscillation potential produced smaller currents than the driven probe in previous experiments, so higher averaging was required to measure *clean* signals. Also, the increased averaging made the scan times longer so plasma stability was an issue. The fact that the oscillation potential was small and the bias voltage increments relatively large meant that the plasma oscillation potential could not be resolved accurately.
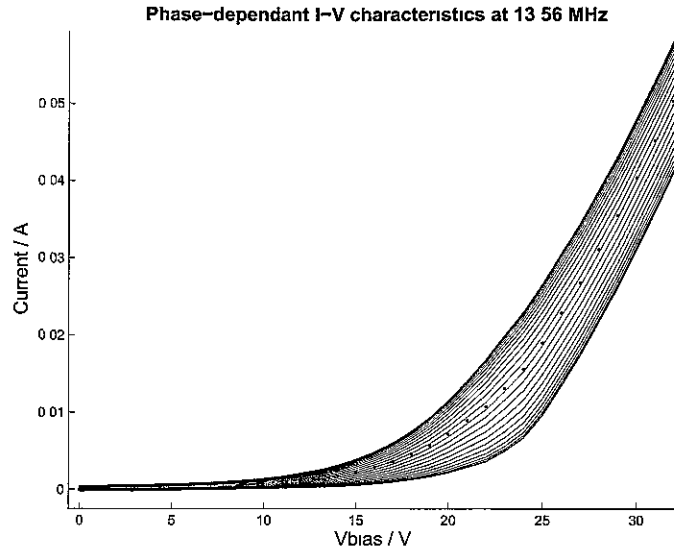
**Figure 6.16:** *Experimental 13 56 MHz phase-dependant I-V characteristics. The dots represent the effective dc characteristic, measured with a compensated probe.*

Similar looking results are obtained in the model when the amplitude of the harmonics are artificially reduced. This suggests that the harmonics in the high frequency experimental case are somehow less than expected. The reason for this is the fact that the capacitive displacement current across the sheath increases as a function of frequency, thus swamping out the desired harmonic content of the conduction current to the probe. At lower frequencies this is not a major issue, but at 13.56MHz the capacitive coupling across the sheath is significant. The time-averaged displacement current is zero, however, because we are looking at the phase-dependant current, it causes some distortion of the measurements.

It is possible to separate the conduction and displacement currents to the probe by measuring the rf voltage, current and phase, as shown by [51] and [49]. However, due to time constraints this has not been attempted yet for these particular measurements. It can only be assumed at this point

that separating the currents will reveal the true conduction current and the associated harmonics, thus allowing this technique to be used accurately at high frequencies.

## 6.2 Summary of Experimental Results

The results clearly demonstrate the validity of the technique, particularly at low frequency where the ions can still respond to the oscillation of the sheath. At higher frequencies, the exact behaviour cannot be predicted by the model, but it was expected that, for reasons given earlier, the theory should still be valid. This appears to be true, as excellent experimental compensation was achieved beyond 10MHz, using only the $f_2(V)$ amplitude.

Almost all of the data recorded showed excellent results in the exponential region, but sometimes deviated from the ideal beyond this. Even so, the deviation is not excessive and at least some level of correction is still maintained in the electron saturation region of the curve. Thus, using $I_{ave}(V)$ - $\Delta I(V)$ allows the correct dc characteristic to be determined. The results are therefore in excellent agreement with the theory.

The phase-dependant results show that, infact, it is un-necessary to measure the individual harmonics, as $\tilde{I}_{RF_{meas}}(V, \tilde{V}_{sh}, \phi) + I_{ave} = \tilde{I}_{total}(V, \tilde{V}_{sh}, \phi)$. This is the most important aspect of this work, as it clearly shows that phase-dependant characteristics can be obtained in an extremely simple manner. This method is both simpler and more powerful than the originally proposed method of summing the harmonic amplitudes to measure $\Delta I$.

Unfortunately, the data-sets were too noisy to accurately recreate the plasma oscillation waveform or to accurately measure phase-dependant parameters, such as, $T_e(\phi)$, $n_e(\phi)$ and $f(E, \phi)$. Greater averaging is needed and

also smaller bias voltage steps. Both of which were reduced to decrease the scan times in the hope of a more stable operating window. A faster more accurate set-up would eliminate these issues, thus providing a very powerful plasma diagnostic.

# CHAPTER 7

---

## Conclusions

---

In this final chapter, the experimental results will be discussed and conclusions drawn about the use of this new technique. This leads on to a discussion on further work and development of the technique for improved results and new areas of investigation

## 7.1 Analysis of Results

Overall the results are in good agreement with the theory presented in the earlier chapters. From the original work of Sloane and McGregor[37], and those who developed their ideas further, it was initially expected that the technique might only work at low frequency, where the ions can respond. This perception comes about because the a.c. superimposed technique relies on low frequencies and small oscillation amplitudes. From our analysis, it is

clear why this is the case - the second harmonic is composed of contributions from the other even harmonics, so only approximates the second derivative when these other terms are small, i e. for small oscillation amplitudes. The characteristic is assumed not to change *shape* as a function of phase, but as frequency increases this may not be true due to the non-linear sheath capacitance. In our analysis, it was assumed that this frequency limit is irrelevant because no matter which component acts non-linearly, or what form the characteristic takes at each point in phase, the resultant distortion, $\Delta I$, must always be reflected in the harmonic amplitudes. The results at higher frequencies (beyond the ion resonance frequency), suggest that this may be true. Excellent compensation of the distorted characteristic was achieved at frequencies over 10 MHz.

The ion resonance was shown to have a strong distorting effect on the measured harmonics. In most plasma systems, the plasma oscillation frequency is generally above the ion resonance so this effect should not be an issue for most researchers. The resonance effect was also investigated to determine if it is possible for the time-averaged values to be decoupled from the harmonic amplitudes, or alternatively if there is some other factor that causes the rectified current to change anomalously with frequency. These results are inconclusive but suggest that in ion resonance the time-averaged values may be *de-coupled* from the sum of *even* harmonic amplitudes, particularly for bias voltages above the dc plasma potential. It is still unclear if this is a real effect or just an experimental artifact.

In the exponential region of the $\Delta I$ curve, the analysis appears to be accurate at all frequencies, but as the plasma potential is approached and exceeded, the deviation from the ideal, or actual $\Delta I(V)$ curve, is more pronounced. It is difficult to find a theoretical explanation for this but may be

due to experimental issues, such as, a result of plasma depletion near electron saturation.

Eventhough the actual $\Delta I(V)$, i.e. $I_{ave}(V) - I_{DC}(V)$, was not replicated precisely by the $f_2(V)$ amplitude over the entire bias range, in all cases, applying $f_2(V)$ as a form of compensation resulted in significantly less distortion, and therefore, much more accurate results. Also, it should be pointed out that to determine the accuracy of this technique, an accurate dc measurement is necessary for comparison. If this measurement is even slightly in error, it will make the $f_2(V)$ measurements appear incorrect.

Clearly, at high frequency the resultant measured waveforms are entirely due to electron current. The effect of this is assumed to be negligible because the ion current is so small in comparison to the electron current. Also, it is known that the time-averaged effect of an oscillation has less influence near ion saturation, where the curve is more linear. Outside of ion saturation the electron current dominates, so the error in neglecting ion current is expected to be small.

The simulations also show that whether or not the ion current is included has little effect on $\Delta I(V)$, however, because the model does not replicate the true effects of frequency on the I-V characteristic, it may be worth further investigation as to what extent ion current has an effect. Nonetheless, the results show excellent compensation ability even at high frequencies, so the assumption of negligible ion current effect seems valid, at least for the frequencies and amplitudes tested.

The amplitude of oscillation for most of the experimental results was 10V amplitude. This is relatively low, at just over a factor of 2 times the average $T_e$. This is probably why the second harmonic alone was sufficient to achieve good compensation. The fourth harmonic was usually found to be negligible.

However, the simulation shows that the forth harmonic *is* significant under approximately the same conditions. This discrepancy may arise because of the difficulty in simulating an exact experimental characteristic. A more accurate comparison between the experiment and simulation could be achieved by applying a fitting curve to the experimental trace and using this *shape* in the simulation. This would reveal if the measured signals are the same as those predicted by theory. The code needs to be modified slightly before this can be attempted.

## 7.2    Experimental Set-up and Simulation

Firstly, the simulation, although simply constructed from basic analytical equations, has proven to be an invaluable and powerful tool. Many of the ideas and developments presented in this thesis would not have been discovered without the aid of the simulation. Developing a more sophisticated model to include the actual effect of frequency and the non-linear capacitance would require a detailed theory of the high frequency sheath around a small probe. This is a far more difficult task.

The experimental set-up was also proven to be fairly effective. The lock-in amplifier, in particular, allowed relatively easy measurement of the second harmonic amplitudes as a function of bias voltage. This set-up also allowed the frequency and amplitude of the oscillation to be varied. This was crucial to proving the validity of the technique.

Measuring the rf waveforms with the current sensor and oscilloscope was found to be more difficult than expected, but almost all these difficulties were caused by the particular equipment used. The averaging was sufficient to provide relatively accurate waveform data, however, this was quite slow

and resulted in scans that usually lasted over 3 minutes. For smaller voltage steps, sufficient to recreate the plasma oscillation, the time required per scan was excessive.

Aside from possible errors caused by changing plasma conditions over time, there may be distortion problems at or above the plasma potential due to electron depletion around the probe tip. Because of the long scan times, the probe must draw saturation current for a relatively long period. With the low plasma densities of this system, depletion is a definite possibility, particularly for larger tip sizes. Using a separate floating probe, a slight change in plasma potential was observed as electron saturation was approached. However, the difference was not excessive. More accurate measurements are required to determine if this is a source of significant error.

Using the equipment available, the maximum amplitude of oscillation during automated data collection was 10 V. For future investigations this should be increased to levels observed in capacitive discharges. Applying the technique to a plasma that is known to have a large oscillation potential would be beneficial as it would eliminate problems caused by driving the probe with a.c., however in this case, frequency and amplitude effects could not be explored as easily.

## 7.3 Phase-Dependant Measurements

Although phase seems like an arbitrary parameter, the simulation shows that it has a significant effect on the analysis, particularly when more than one harmonic is used for the $\Delta I(V)$ reconstruction. The mathematical analysis also shows that although the magnitudes of the even harmonics may be independent of phase, their sum is not. Reconstructing the exact $\Delta I(V)$

curve is thus more difficult than theory predicts, but it is possible. Also, the discovery that the (t = 0) curve of the rf I-V characteristic gives $\Delta I(V)$ exactly is extremely important, as it simplifies the problems with measuring harmonics individually.

Another important and interesting point is that the $\Delta I(V)$ curve obtained at t=0 from the rf I-V characteristic of figure (6.12), shows no obvious sign of distortion due to resonance. When $f_2(V)$ is measured at the same frequency (200 kHz) under the same conditions, a clear resonance effect is observed. Thus, it is clear that the effect of resonance is not well understood in terms of this technique. Having said that, in general, the resonance condition can be be avoided so should not represent a problem in commercial plasma systems.

Of most importance is the fact that, for the first time, complete phase-dependant characteristics are obtainable in a simple manner, at least for frequencies less than 13.56MHz. The traditional langmuir probe circuit requires only the addition of a synchronized rf current sensor to record phase resolved I-V characteristics. Studying the phase-dependant nature of the characteristic may help develop more accurate theories of probe behaviour in rf plasma, and ultimately a better understanding of plasma behaviour in general.

At higher frequencies the effect of the displacement current must be taken into account and/or removed. It should also be noted that it is unclear how the non-linear capacitance of the sheath will affect the displacement current. This must also be considered. More measurements are needed.

# 7.4   Further Possibilities

Many new possibilities arise from this work, some of these are presented here:

### Commercial System:

The experimental methods presented were found to be adequate for demonstrating the ideas and techniques developed, however, there were many issues with accuracy. A specific system designed purely for measuring the the rf data and generating the rf I-V characteristics would be fairly simple to implement. Accurate FFT's could be generated at the current sensor itself, while a digital output from this could be analysed by on-board software. This would allow rapid scans and much higher averaging capabilities. Accurate comparison of the phase-dependant parameters should then be possible, even at very high frequencies beyond which existing methods are capable of measuring.

### Second Harmonic *Only* Compensation:

In many situations, rf inductors will still be required to prevent the rf signals from reaching the bias supply and also to prevent the rf current flowing through the probes low impedance to ground. It has been shown that the magnitude of $\Delta I(V)$ is a function of the oscillation potential, therefore, measuring the $f_2(V)$ amplitude of any compensated probe will reveal exactly how 'compensated' it really is. Clearly, if $f_2(V) << I_{ave}$, then the compensation must be sufficient. Thus, $f_2(V)$ can be used as a validator for fully compensated probes. Subtracting the measured $f_2(V)$ signal will further increase the probes compensation ability if necessary.

This may be extended further by looking at how traditional compensation works in the first place. The inductors essentially block the fundamental, which would otherwise cause oscillation of the sheath current. It is this os-

**114**

cillation that causes the time averaged distortion, so the inductors attempt to cut off the sheath oscillation at the source. This requires that the inductor impedance be much larger than the sheath impedance, which is difficult to achieve and was one of the main reasons for this work. However, as the harmonic analysis shows, only the *even* order harmonics are capable of creating a non-zero time-averaged value, therefore, the sheath *can* oscillate without causing distortion, as long as the *even* harmonics are removed. At first, this may seem like a trivial substitution, as now we need to block the second harmonic (mainly) as opposed to the first, however this has its advantages. Because the second harmonic is twice the fundamental frequency, its impedance at the sheath is halved. So immediately, the required inductor impedance is reduced significantly (by around 10 times)

Usually, when multi-harmonic compensation is used on a probe, the idea is to block all the oscillating components in the plasma oscillation, such as, fundamental($f_1$) and second harmonic($f_2$) of the driving frequency. However, the simulation shows that for non-sinusoidal inputs, the higher *even* order harmonics of *all* the input signal frequencies are needed. This has never been seen in the literature. The apparent success of multi-harmonic compensation is then mainly due to the fact that the second harmonic of the fundamental contains many of the higher *even* order contributions.

This compensation will therefore be insufficient when the ratio of $(f_2/f_1)$ increases. A large second harmonic component in the plasma oscillation will therefore require significant impedance at the $4^{th}$ and $6^{th}$ harmonics. This suggests that rf compensation is even more complicated than previously expected, especially when the plasma oscillation is non-sinusoidal, which is often the case. The technique presented in this thesis is therefore a significant simplification.

**Ultra-Thin Probes:**

Because traditional rf compensation techniques may be eliminated by this technique, it opens the possibility of using probes with an extremely small cross-section. Electrostatic probes will always be invasive, however, the smaller the probe, the smaller the disturbance to the plasma. The probe dimensions are only limited in this case by the accuracy of the measurement system, as the probe currents may be much smaller than usual.

## 7.5 Final Summary

Overall the experimental results show excellent agreement with the simple mathematical model and simulated results. The theory predicts, and the experimental results show, that the time-averaged distortion component, $\Delta I$, can for the first time be separated from the total measured current of an uncompensated (or insufficiently compensated) electrostatic probe in a radio-frequency plasma. The distortion to the resultant I-V characteristic can thus be removed, restoring the correct values of the calculated plasma parameters. This is achieved in a relatively simple manner, without the need for complex rf compensation methods. Frequency and amplitude do not appear to be limiting factors, as with other methods, so this technique should work in situations where *normal* rf compensation is a practical impossibility.

The fact that important dc information is retained eventhough the rf current is measured through a blocking capacitor, is both surprising and extremely useful. The phase-dependant nature of the characteristic can thus be obtained in a simple way.

Since the Langmuir probe was invented, over 80 years ago, its main attraction has been the simplicity of its design and the wealth of information it is capable of retrieving. However, since the advent of radio-frequency discharges, the simplicity of the probe itself has been lost along the way and more complex methods and systems have been developed to overcome its inherent problems. The work in this thesis shows that the simplest of probes *can* actually be used in situations where it was previously disregarded, but also, can now be extended to create an even more powerful diagnostic technique.

# Bibliography

[1] Irving Langmuir. The collected works of irving langmuir. *Pergamon Press Ltd, New York*, Vol. 5, 1961.

[2] H.M.Mott-Smith I.Langmuir. *Gen.Elec.Rev.*, 26:731, 1923.

[3] H.M.Mott-Smith and I.Langmuir. Theory of collectors in gaseous discharges. *phys.rev.*, 28:727, 1926.

[4] F.F.Chen. Lecture notes on the principals of plasma physics. *Book*, Part A7, 2003.

[5] F F.Chen. Saturation ion currents to langmuir probes. *J. Appl. Phys.*, 36:675–678, 1965.

[6] M.B.Hopkins. Langmuir probe measurements in the gaseous electronics conference rf reference cell. *J. Res. Natl. Inst. Stand. Technol.*, 100: 415–425, 1995.

# BIBLIOGRAPHY

[7] M.B.Hopkins and W.G.Graham. Langmuir probe technique for plasma parameter measurement in a medium density discharge. *Rev. Sci. Instum.*, 57:2210–2217, 1986.

[8] R.B.Piejak V.A.Godyak and B.M. Alexandrovich. Probe diagnostics of non-maxwellian plasmas. *J.Appl.Phys.*, 73, 1992.

[9] M.A.Lieberman and A.J Lichtenberg. Principals of plasma discharges and materials processing. *Wiley*, Second Edition, 2005.

[10] I.Sudit and R.C.Woods. A study of the accuracy of various langmuir probe theories. *J. Appl. Phys.*, 76:4488–4498, 1994.

[11] J.G.Laframboise. Theory of spherical and cylindrical probe langmuir probes in a collisionless maxwellian plasma at rest. *Institute of aerospace studies, Toronto, Canada*, 100, 1966.

[12] C.Steinbruchel. *J. Vac Sci. Technol*, 8:1663, 1990.

[13] Shih and levi. Effect of collision on cold ion collection by means of langmuir probe. *AIAA Journal*, 9:1673–1680, 1971.

[14] M.W. Allen B.M. Annaratone and J.E. Allen. Ion currents to cylindrical probes in rf plasmas. *J.Phys. D : Appl. Phys.*, 25:417–424, 1992.

[15] J.E.Allen. Probe theories and applications: modern aspects. *Plasma Sources Sci. Technol*, 4:234–241, 1994.

[16] V.Pletnev and J.G.Laframboise. Current collection by a cylindrical probe in a partly ionized collisional plasma. *Physics of Plasmas*, 13: 073503-1 – 073503-19, 2006.

[17] S.V.Ratynskaia V.I.Demidov and K.Rypdal. Electric probes for plasmas: The link between theory and instrument. *Rev. Sci. Intrum.*, 73:3309–3439, 2002.

[18] P.C.Strangby. *Phys. Fluids*, 27:2699, 1984.

[19] Yu.M.Kagan and V.I.Perel. *Sov.Phy. Usp.*, 6:767, 1964.

[20] R.B.Piejak V.A.Godyak and B.M. Alexandrovich. Measurement of electron energy distribution in low-pressure rf discharges. *Plasma Sources Sci. Technol.*, 1:36–58, 1992.

[21] Oksuz and Soberon. Uncompensated probes revisited. 2005.

[22] M.Hannemann and F. Sigeneger. Langmuir probe measurements at incomplete rf-compensation. *Czech J. Phys.*, 56, 2006.

[23] R.R.J.Gagne and A.Cantin. *J. Appl. Phys.*, 43.2639, 1972.

[24] V.A.Godyak and R.B.Piejak. Probe measurements of the space charge potential in an rf discharge. *J. Appl. Phys.*, 68:3157–3162, 1990.

[25] I.D.Sudit and F.F.Chen. Rf compensated probes for high density discharges. *Plasma Sources Sci Technol.*, 3:162–168, 1994.

[26] A.E.Wendt. Passive external rf filter for langmuir probes. *Rev. Sci. Instrum*, 72:2926–2930, 2001.

[27] John Scanlan. Langmuir probes in 13.56 mhz discharges. *PhD Thesis, Dublin City University*, 1991.

[28] N.M.P.Benjamin N.St.J.Braithwaite and J.E. Allen. An electrostatic probe technique for rf plasma. *J. Phys. E: Sci. Instrum.*, 20:1046–1048, 1987.

[29] A.Dyson P.Bryant and J.E.Allen. Multiple harmonic compensation of langmuir probes in rf discharges. *Meas. Sci. Technol.*

[30] F.W.Crawford. Modulated langmuir probe characteristics. *J. Appl. Phys.*, 34:1897–1902, 1962.

[31] A.Boschi and F.Magistrelli. *Nuovo Cimento*, 29.487, 1963.

[32] Garscadden and Emeleus. Notes on the effect of noise on langmuir probe characteristics. *Proc. Phys. Soc*, 79, 1962.

[33] F.F.Chen. Time-varying impedance of the sheath on a probe in an rf plasma. *Plasma Sources Sci. Technol.*, 15:773–782, 2006.

[34] N. Hershkowitz. Plasma diagnostics. *Boston Academic*, Vol.1 chapter 4, 1989.

[35] P.A.Sturrock. Microwave laboratory report no.638. *W. W.Hansen Laboratories of Physics, Stanford University*, 1958.

[36] H.S.Butler and G.S.Kino. Plasma sheath formation by radio frequency fields. *Physics of Fluids*, 6:1346–1355, 1963.

[37] R.H.Sloane and E.I.R.McGregor. *Phil. Mag.*, 18.193–207, 1934.

[38] R.P.Jones A.I.Kilvington and J.D.Swift. Effect of a.c. amplitude on the measurement of electron energy distribution functions. *J Sci. Instrum*, 44:517–520, 1967.

[39] R L F Boyd and N.D. Twiddy. *Proc. Royal Soc. A*, 250:53–69, 1959.

[40] Felipe Soberon Vargas Prada. Plasma transport and development of plasma kinetics ion aris. *PhD Thesis, Dublin City University*, 2005.

[41] K.Takayama and H.Ikegami. Plasma resonance in a radio frequency probe. *Phys. Rev. Letters*, 5:238, 1960.

[42] T. Dote and T.Ichimiya. Characteristics of resonance probes. *J. Appl. Phys.*, 36:1866, 1964.

[43] R.S.Harp and F.W.Crawford. Characteristics of the plasma resonance probe. *J. Appl. Phys.*, 35, 1964.

[44] R.Rosa. Ion transit time effects in the plasma sheath. *J. Phys. A: Gen. Phys.*, 4:934–943, 1971.

[45] B.M.Oliver, R.M.Clements, and P R.Smy. Experimental investigation of the low frequency capacitive response of a plasma sheath. *J Appl. Phys.*, 44:4511–4517, 1973

[46] J. Felsteiner Yu.P.Bliokh and Ya.Z.Slutsker. Resonance instability of the non-steady state plasma sheath. *J. Plasma. Phys*, 2005.

[47] Hiroshi Amemiya and Kazuo Shimizu. Frequency dependance of the alternating current method for measuring the electron energy distribution function in plasmas. *J. Phys. E: Sci. Instrum*, 12:581–583, 1979.

[48] J. Felsteiner Yu.P.Bliokh and Ya.Z.Slutsker. Existance and stability of the plasma sheath resonance near the ion plasma frequency. *EuroPhys. Lett.*, 46:735–740, 1999.

[49] David Gahan. Radio frequency discharge power measurement with emphasis on collisionless electron heating in capactive sheaths. *PhD Thesis, Dublin City University*, 2006.

[50] M. A. Sobolewski. Measuring the ion current in electrical discharges using radio-frequency current and voltage measurements. *Applied Physics Letters*, 72:1146, 1998.

[51] M. A. Sobolewski. Electrical characteristics of argon radio frequency glow discharges in an asymmetric cell. *IEEE trans. plasma Sci.*, 23, 1995.